



HAL
open science

Clinical and neuropathological diversity of tauopathy in MAPT duplication carriers

David Wallon, Susana Boluda, Anne Rovelet-Lecrux, Manon Thierry, Julien Lagarde, Laetitia Miguel, Magalie Lecourtois, Antoine Bonnevalle, Marie Sarazin, Michel Bottlaender, et al.

► **To cite this version:**

David Wallon, Susana Boluda, Anne Rovelet-Lecrux, Manon Thierry, Julien Lagarde, et al.. Clinical and neuropathological diversity of tauopathy in MAPT duplication carriers. *Acta Neuropathologica*, 2021, 142 (2), pp.259-278. 10.1007/s00401-021-02320-4 . hal-03357184

HAL Id: hal-03357184

<https://normandie-univ.hal.science/hal-03357184v1>

Submitted on 30 Jul 2024

HAL is a multi-disciplinary open access archive for the deposit and dissemination of scientific research documents, whether they are published or not. The documents may come from teaching and research institutions in France or abroad, or from public or private research centers.

L'archive ouverte pluridisciplinaire **HAL**, est destinée au dépôt et à la diffusion de documents scientifiques de niveau recherche, publiés ou non, émanant des établissements d'enseignement et de recherche français ou étrangers, des laboratoires publics ou privés.

[Click here to view linked References](#)

1 **Clinical and neuropathological diversity of tauopathy in *MAPT* duplication**
2 **carriers**

3 David Wallon^{1,*}, Susana Boluda^{2,3*}, Anne Rovelet-Lecrux⁴, Manon Thierry^{2,3},
4 Julien Lagarde^{5,6}, Laetitia Miguel⁴, Magalie Lecourtois⁴, Antoine Bonneville¹, Marie
5 Sarazin^{5,6}, Michel Bottlaender^{6,7}, Mathieu Mula³, Serge Marty², Natsuko Nakamura²,
6 Catherine Schramm³, François Sella⁸, Thérèse Jonveaux⁹, Camille Heitz¹⁰, Isabelle Le
7 Ber¹¹, Stéphane Epelbaum¹², Eloi Magnin¹², Aline Zarea¹, Stéphane Rousseau⁴, Olivier
8 Quenez⁴, Didier Hannequin¹, Florence Clavaguera², Dominique Campion⁴, Charles
9 Duyckaerts^{2,3}, Gaël Nicolas⁴

10

11 *¹Normandie Univ, UNIROUEN, Inserm U1245, CHU Rouen, Department of Neurology and*
12 *CNR-MAJ, F 76000, Rouen, France*

13 *²Sorbonne Université, INSERM, CNRS U1127, Institut du Cerveau, ICM, Paris, France*
14 *Sorbonne Université, INSERM, CNRS U1127, Institut du Cerveau, ICM, Paris, France*

15 *³AP-HP, Hôpital de la Pitié-Salpêtrière, Laboratoire de Neuropathologie R. Escourolle, Paris,*
16 *France.*

17 *⁴Normandie Univ, UNIROUEN, Inserm U1245, CHU Rouen, Department of Genetics and*
18 *CNR-MAJ, F-76000 Rouen, France*

19 *⁵Unit of Neurology of Memory and Language, GHU Paris Psychiatry and Neurosciences,*
20 *Hôpital Sainte Anne, F-75014, Paris & Université de Paris, F-75006 Paris*

21 *⁶Université Paris-Saclay, BioMaps, CEA, CNRS, Inserm, F-91401, Orsay, France*

22 *⁷UNIACT, Neurospin, CEA, 91191, Gif-sur-Yvette, France*

23 *⁸Department of Neurology, Hôpitaux Civils de Colmar and INSERM U-1118, School of*
24 *Medicine, Strasbourg University, France*

25 *⁹CMRR Department of Neurology, Nancy University Hospital, Laboratoire Lorraine de*
26 *Psychologie et de Neurosciences de la Dynamique des Comportements 2LPN EA7489 Lorraine*
27 *University, Nancy, France*

1 ¹⁹Neurology Department, Hôpital Universitaire de Nîmes, Nîmes, France

2 ¹¹Sorbonne Université, Paris Brain Institute – Institut du Cerveau – ICM, Inserm U1127, CNRS
3 UMR 7225, AP-HP - Hôpital Pitié-Salpêtrière, Paris, France & Reference Centre for Rare or
4 Early Dementias, IM2A, Département de Neurologie, AP-HP - Hôpital Pitié-Salpêtrière, Paris,
5 France

6 ¹²Centre Mémoire Ressources et Recherche (CMRR), Centre Expert Parkinson (CEP), service
7 de Neurologie, CHRU Besançon, F-25000 Besançon, France & Neurosciences intégratives et
8 cliniques UR481, Univ. Bourgogne Franche-Comté, F-25000 Besançon, France

9

10 *equal contribution

11

12 **Corresponding Authors:**

13 David Wallon, department of Neurology, Rouen University Hospital, 37 boulevard Gambetta,
14 76031 Rouen cedex, tel.: 0033 2 32 88 58 01, email: david.wallon@chu-rouen.fr

15 Gaël Nicolas, department of Genetics, Rouen University Hospital, 37 boulevard Gambetta,
16 76031 Rouen cedex, tel.: 0033 2 32 88 80 80, email: gaelnicolas@hotmail.com

17

18 **ACKNOWLEDGEMENTS**

19 Two of the neuropathological cases described in this paper (ALZ_441_005 and ALZ_596_006)
20 have been collected by the Neuro-CEB brain bank, Paris, France.

21 We thank Luc Buée for helpful advices and Gabor Kovacs for sharing unpublished data.

22 This work was supported by Fondation pour la Recherche Médicale (Equipe FRM
23 DEQ20170336711).

24 We thank the technical team at Raymond Escourolle neuropathology department. We thank the
25 ICM-Quant core facility, Paris Brain Institute (ICM).

26

1 **Disclosures:**

2 The authors have nothing to disclose in relation to this article.

3

1 ABSTRACT:

2 Microduplications of the 17q21.31 chromosomal region encompassing the *MAPT* gene, which
3 encodes the Tau protein, were identified in patients with a progressive disorder initially
4 characterized by severe memory impairment with or without behavioral changes that can
5 clinically mimic Alzheimer disease. The unique neuropathological report showed a primary
6 tauopathy, which could not be unanimously classified in a given known subtype, showing both
7 4R- and 3R-tau inclusions, mainly within temporal cortical subregions and basal ganglia,
8 without amyloid deposits. Recently, two subjects harboring the same duplication were reported
9 with an atypical extrapyramidal syndrome and gait disorder. To decipher the phenotypic
10 spectrum associated with *MAPT* duplications, we studied 10 carriers from 9 families, including
11 2 novel unrelated probands, gathering clinical (n=10), cerebrospinal fluid (N=6), MRI (n=8),
12 dopamine transporter scan (n=4), functional (n=5), amyloid (n=3) and Tau-tracer (n=2) PET
13 imaging data as well as neuropathological examination (n=4). Ages at onset ranged from 37 to
14 57 years, with prominent episodic memory impairment in 8/10 patients, associated with
15 behavioral changes in four, while two patients showed atypical extrapyramidal syndrome with
16 gait disorder at presentation, including one with associated cognitive deficits. Amyloid imaging
17 was negative but Tau imaging showed significant deposits mainly in both mesiotemporal
18 cortex. Dopaminergic denervation was found in 4/4 patients, including three without
19 extrapyramidal symptoms. Neuropathological examination exclusively showed Tau-
20 immunoreactive lesions. Distribution, aspect and 4R/3R tau aggregates composition suggested
21 a spectrum from predominantly-3R, mainly cortical deposits well correlating with cognitive
22 and behavioral changes, to predominantly-4R deposits, mainly in the basal ganglia and
23 midbrain, in patients with prominent extrapyramidal syndrome. Finally, we performed *in vitro*
24 seeding experiments in HEK-biosensor cells. Morphological features of aggregates induced by
25 homogenates of three *MAPT* duplication carriers showed dense/granular ratios graduating
26 between those induced by homogenates of a Pick disease and a progressive supranuclear palsy
27 cases. These results suggest that *MAPT* duplication causes a primary tauopathy associated with
28 diverse clinical and neuropathological features.

29

30 **Keywords:** tau, MAPT duplication, progressive supranuclear palsy, Pick disease, Tau seeding.

1 INTRODUCTION

2 The *MAPT* gene encodes tau, a microtubule binding protein, which forms pathological cellular
3 aggregates in several neurodegenerative disorders termed tauopathies [14, 20]. In primary
4 tauopathies, tau is the driving pathological factor whereas in secondary tauopathies such as
5 Alzheimer Disease (AD), the pathological process is associated with the interaction of tau with
6 other proteins or peptides, namely the A β peptide in AD. Additionally, tauopathies can be
7 divided into 3R, 4R or mixed subtypes according to the isoforms that accumulate. The *MAPT*
8 messenger RNA can be alternatively spliced resulting in 6 isoforms of the tau protein. 4R-tau
9 refers to tau isoforms including 4 microtubule-binding repeats whereas 3R-tau includes only 3
10 repeats due to the splicing out of *MAPT* exon 10 [14].

11 The 17q21.31 microduplication is a rare recurrent rearrangement involving four genes (*CRHRI*,
12 *MAPT*, *STH* and *KANSL1*) which causes a recently recognized neurodegenerative disorder with
13 poorly defined phenotypic features [15]. Among the first few cases initially reported, a constant
14 clinical feature was severe memory impairment, associated in some cases with behavioral
15 changes leading either to a clinical diagnosis of typical Alzheimer disease (AD) phenotype or
16 behavioral variant of Alzheimer disease [1, 12, 15, 21]. In a previous report, we found that the
17 cerebrospinal (CSF) biomarkers profile of the 17q21.31 duplication was consistent with an AD
18 diagnosis in 3/4 patients, including tau-related neurodegenerative processes and abnormal
19 amyloid β (A β) levels. However, amyloid positron emission tomography (PET) imaging did
20 not support this conclusion [15]. So far, detailed neuropathological examination has been
21 published only for one patient [1]. This case showed a marked atrophy of the frontal and the
22 temporal lobes, hippocampus, amygdala, and a depigmentation of the substantia nigra.
23 Immunostaining for A β and α -synuclein remained negative in all regions examined. The most
24 prominent neuropathological alterations were 4R-tau inclusions, although 3R-tau positive
25 neurofibrillary tangles were also observed in the hippocampus, entorhinal cortex, striatum,
26 nucleus basalis of Meynert and substantia nigra. Despite its clinical presentation and CSF
27 biomarkers profile in some patients, the 17q21.31 duplication thus appears to cause a pure
28 tauopathy. The main pathophysiological mechanism associated with this duplication is a 1.6-
29 1.9 fold increase of the *MAPT* messenger RNA as measured in blood samples of duplication
30 carriers [15], presumably increasing tau protein levels. To further complicate the matter, it has
31 recently been reported that this duplication was present in two subjects clinically diagnosed
32 with a different phenotype, *i.e.* atypical extra-pyramidal syndrome with gait disorder [4].
33 However, the in-depth description of neuropathological findings in those last two cases was not
34 reported. In the present article, we describe novel cases, reanalyze the previously published

1 cases with additional imaging and CSF data and report the detailed results of four
2 neuropathological examinations.

3

4 **METHODS**

5 **Cases**

6 Eight demented cases with an *MAPT* microduplication collected from year 2009 to year 2019
7 by our laboratory were studied. Six cases were previously published [15, 21]. For two of those
8 six cases, we add here neuropathological data that were not available at the time and updated
9 clinical and paraclinical information. Two additional unpublished cases were identified in the
10 meantime and added to this series. Finally, two cases, enrolled in a series of extrapyramidal
11 syndromes, were previously published without neuropathological details [4], which we are
12 providing here.

13 All patients (or legal representatives) gave informed, written consent for genetic analyses. All
14 patients underwent a comprehensive clinical examination including personal medical and
15 family history, neurological examination, neuropsychological assessment and, for some,
16 lumbar puncture with CSF biomarkers analysis. Structural Magnetic Resonance Imaging
17 (MRI), ¹²³I-Ioflupane Dopamine Transporter Single Photon Emission Computerized
18 Tomography (Datascans) and ¹⁸Fluro-deoxy-glucose (FDG) Positon Emission Tomography
19 (PET) or single-photon emission computed tomography (SPECT) with hexa-methyl-propylene-
20 amine-oxime (HMPAO) imaging were collected when performed as well as Amyloid and Tau-
21 PET cerebral imaging (see details below). We collected clinical and paraclinical information
22 from medical charts of all participants. Autopsies for cases were performed with the
23 authorization of the patient himself or the next of keen. Cases ALZ_441_005 and
24 ALZ_596_006 were obtained through the French national brain bank network, Neuro-CEB. We
25 certify that the study was performed in accordance with the ethical standards as laid down in
26 the 1964 Declaration of Helsinki and its later amendments.

27

28 **Genetic analyses**

29 Copy Number Variants (CNVs) were identified from whole exome sequencing data and
30 confirmed by quantitative multiplex PCR of short fluorescent fragments (QMPSF) as
31 previously described [15], except for the two additional cases identified by DNA chips (SNP
32 array genotyping) and validated by qPCR [4]. H1/H2 *MAPT* haplotypes genotyping was
33 determined by SNaPshot experiments using the rs1052553 single nucleotide polymorphism as
34 a tag. Sub-haplotypes could not be determined because, in most individuals, it was not possible

1 to unambiguously phase the polymorphisms used to tag these sub-haplotypes.
2 Exon 10 and at least 20 bp of the surrounding splicing regions were re-sequenced with the
3 Sanger technique using specific primers (available upon request).

5 **CSF biomarker analysis**

6 CSF biomarker analyses were carried out in 6 different laboratories as part of the diagnostic
7 workup using a standardized procedure. CSF samples were obtained using a Sprotte needle and
8 collected in polypropylene tubes. They were aliquoted after centrifugation into polypropylene
9 Eppendorf tubes, then frozen at -80°C within 1 h. $\text{A}\beta_{42}$, Tau (total-tau protein), and P-Tau
10 (phosphorylated-tau protein in position 181) measurements were performed using an enzyme-
11 linked immunosorbent assay (ELISA) (Fujirebio) according to the manufacturer's instructions.
12 The analysis of all biomarkers was performed in two runs and averaged for statistical analyses.
13 The quality of the results was ensured by the use of validated standard operating procedures
14 and internal quality controls (QC) as all centers were already involved in nationwide studies.
15 The following cut-offs were used: $\text{A}\beta_{42} < 550 \text{ pg/mL}$, Tau $> 350 \text{ pg/mL}$, P-Tau $< 60 \text{ pg/mL}$. When
16 $\text{A}\beta_{40}$ was available, the normal $\text{A}\beta_{42}/\text{A}\beta_{40}$ ratio cut-off was > 0.05 .

18 **Cerebral Imaging Data**

19 When available, MRI scans were assessed using native DICOM format images. The presence
20 of a cortical atrophy was evaluated; hippocampal atrophy was bilaterally scored following
21 Scheltens visual rating scale [24]. Cortical functional imaging was assessed to identify focal
22 hypometabolism using ^{18}F FDG-PET or hypoperfusion using HMPAO-SPECT. Available
23 DaTscan interpretations of trained nuclear physicians were used to confirm or identify
24 dopaminergic denervation.

26 **Amyloid and Tau PET imaging**

27 Amyloid- β PET imaging of three patients was performed using ^{18}F -florbetapir (n=1), ^{18}F -
28 florbetaben (n=1) or ^{18}F -flutemetamol (n=1) as previously described [15]. Tau-PET
29 examination was performed in two patients (and compared to 13 already available control
30 subjects, mean age = 68.8 years [64-75]) on a High-Resolution Research Tomograph (HRRT;
31 CTI/Siemens Molecular Imaging). The acquisition was performed from 80 to 100 minutes after
32 intravenous administration of $382 \pm 11.3 \text{ MBq}$ of ^{18}F -flortaucipir. Dynamic list mode
33 acquisitions were binned into successive 5-minute time frames. Parametric images were created
34 using BrainVisa software (<http://brainvisa.info>) by averaging the original 5-min images over

1 80-100 min after administration of flortaucipir. Standard Uptake Value ratio (SUVr) parametric
2 images were obtained by dividing each voxel by the average value of the cerebellar grey matter
3 region-of-interest with an erosion of 4 mm. Seventy-six cortical volumes of interest (VOI) were
4 defined based on individual MRI scans and then applied onto the subject's PET space following
5 coregistration. The VOIs, defined separately for the left and right hemispheres, were pooled
6 into broader anatomical volumes of interest: we considered three cortical VOIs on the left and
7 right sides respectively encompassing the temporal (with its parahippocampal, fusiform and
8 polar sub-regions), parietal and frontal lobes.

10 **Neuropathological examination**

11 For each autopsy case, one hemisphere was fixed in formalin (fixation times between 8 and 27
12 months) and the contralateral hemisphere was frozen at -80°C, except for case EXT_2000_001
13 in which the whole brain was fixed in formalin. Immunostaining was performed with the
14 Benchmark station automated system (Ventana Medical system Inc., Roche) using the
15 following antibodies: anti-phospho-tau (pS202,pT205): clone AT8 (mouse monoclonal,
16 ThermoFischer, 1/500); anti 3R-Tau (RD3): clone 8E6/C11 (mouse monoclonal, Merck, 1/100);
17 anti 4R-Tau (RD4): clone 1E1/A6 (mouse monoclonal, Merck, 1/50), anti phospho-tau
18 (pT212,pS214): clone AT100 (mouse monoclonal, ThermoFischer, 1/500), anti p-62: clone
19 3/P62 Ick ligand (mouse monoclonal, BD Biosciences, 1/500), anti-A β antibody: clone 6F/3D
20 (mouse monoclonal, Agilent, 1/200); anti-TDP43 (rabbit polyclonal, Proteintech, 1/1,000); anti
21 α -synuclein: clone 5G4 (mouse monoclonal, Millipore, 1/4,000). Except for
22 immunohistochemistry with the A β and p62 antibodies, tissue was pretreated using a buffer at
23 pH8 at 95°C between 8 minutes and 1 hour before adding the antibodies. The antibodies were
24 incubated at 37°C between 32 minutes and 2 hours. The antigen retrieval used for A β was 5
25 minutes in formic acid and incubation of the antibody overnight at room temperature. For p62,
26 the antigen retrieval was done in a buffer at pH_6 for 76 minutes and incubation of the primary
27 antibody for 96 minutes at 37°C. Gallyas and Bielschowsky silver techniques were used to
28 assess argyrophilic properties of tau aggregates [29, 30].

29 A β oligomers were extracted from frontal cortex following Lesné et al. procedures [16] and
30 analyzed by Western blot using WO2 antibody (Covance, Princeton, NJ).

31 Molecular profiles of tau aggregates were analyzed from sarkosyl-insoluble fraction following
32 the protocol described by Sahara and Kimura [22] for patients ALZ_441_005 and ALZ
33 _596_006 using brain samples extracted from frontal cortex and striatum. A patient with Pick's
34 disease (PiD), an AD patient and a control individual were processed in parallel. Sarkosyl-

1 insoluble fractions from patient EXT_1998_001 and a subject with progressive supranuclear
2 palsy (PSP) were obtained following the protocol described by Dan et al [6]. Indeed, the
3 protocol from Sahara and Kimura did not enable us to obtain sufficient amounts of sarkosyl-
4 extractable aggregates for EXT_1998_001. Hence, we observed a slightly different staining for
5 patient EXT_1998_001; notably, the 3R staining revealed several bands from lower molecular
6 weight, which were not observed for the other patients. For the sake of comparison, the AD
7 patient and the control individual were also extracted with this method. Sarkosyl-insoluble
8 fractions were analyzed by Western blot using the following antibodies: anti Phospho-tau
9 (pT181) antibody: AT270 (mouse monoclonal, ThermoFischer, 1/200), anti 3R-Tau (RD3):
10 clone 8E6/C11 (mouse monoclonal, Merck, 1/1,000), anti 4R-Tau (RD4): clone 1E1/A6 (mouse
11 monoclonal, Merck, 1/200).

12

13 **Quantification of the 4R/3R tau ratio from brain mRNA**

14 The mRNA from frontal cortex and striatum of three patients carrying the *MAPT* duplication
15 and 5 normal controls was extracted using RNA extraction kit (Macherey-Nagel). Reverse
16 transcription was performed using verso cDNA kit (ThermoFisher Scientific). Then, cDNAs
17 were PCR-amplified in a limited number of cycles, using a 6-FAM labelled F primer located
18 on exon 9 (5'-CCCAAGTCGCCGTCTTCC-3') and a R primer located on exon 11 (5'-
19 TGGTTTATGATGGATGTTGCCT-3'). This resulted in the amplification of 2 fragments of
20 207 and 300 bp, depending on the exclusion (3R-Tau) or inclusion (4R-Tau) of exon 10,
21 respectively. After migration on an ABIprism 3500 automated sequencer (Applied Biosystems),
22 the peak heights were quantified using the GeneMapper5 software in order to determine the
23 4R/3R Tau ratios.

24

25 **In vitro seeding experiments**

26 Preparation of human brain homogenates. In addition to brain tissues from ALZ_441_005,
27 ALZ_596_006 and EXT_1998_001, three additional *post-mortem* brains, collected in a brain
28 donation project and stored in the French national brain biobank (Bioresource Research Impact
29 Factor number = BRIF BB-0033-00011), were used for this study: one 72-year-old male
30 corresponding to a control case devoid of any A β , phospho-tau or α -synuclein accumulation,
31 one 64-year-old female with progressive supranuclear palsy (PSP case) and one 61-year-old
32 male with Pick's disease (PiD case). The following samples were chosen: striatum of the three
33 *MAPT* duplication cases, pons of the PSP case (as example of a 4R tauopathy) and frontal cortex
34 of the PiD case (as example of a 3R tauopathy). The striatum of the control case was also

1 studied. Approximately 150 mg of frozen tissue were thawed on ice and mixed with ice-cold
2 phosphate-buffered saline (PBS) containing protease and phosphatase inhibitor cocktail
3 (Thermo Fisher Scientific), to reach a final solution of 20% weight/volume. Tissue was
4 homogenized by 15-20 strokes in a 1 mL glass homogenizer (Fisher Scientific), briefly
5 sonicated on ice with a Misonix Q125 sonicator (Q-sonica) and clarified by centrifugation
6 (3000 g, 5 min, 4°C), as previously described [27]. Supernatants were collected, aliquoted and
7 stored at -80°C. Concentrations of tau proteins were assessed by total tau (Total) Human ELISA
8 Kit (Invitrogen, Thermo Fisher Scientific).

9 Treatment of biosensor cells sensitive to tau seeding. The seeding activity of each homogenate
10 was evaluated on a misfolded tau biosensor (HEK cells expressing tau RD P301S coupled with
11 YFP or CFP fluorochromes, #CRL-3275, ATCC, LGC Standards). Those cells were plated in
12 24-well plates and treated in duplicate, following the original protocol adapted at the laboratory
13 [9, 11], with a few adjustments. A transduction mix was prepared with 43.75 µL Opti-MEM
14 (Gibco, Thermo Fisher Scientific) and 6.25 µL Lipofectamine 2000 (Invitrogen, Thermo Fisher
15 Scientific), combined with 50 µl of the homogenate diluted in Opti-MEM and normalized by
16 total tau. The transduction mix was briefly spun, incubated for 30 min at room temperature and
17 added to the cells. Cells were left in the incubator during 24h. The experiment was replicated
18 three times.

19 Analysis. Treated cells were re-plated on 13 mm diameter coverslips coated with poly-D-lysine
20 (Sigma-Aldrich) and left 6-7h in the incubator. Cells were fixed in 4% PFA and counterstained
21 with DAPI. The coverslips were mounted with Fluoromount (Sigma-Aldrich). Slides were
22 stored in the dark at 4°C until observation with an inverted confocal Leica TCS SP8 DLS (Leica
23 Microsystems). The YFP/CFP positive cells were manually counted from max intensity
24 projection images (4 microscopic fields per coverslip, 8 per condition). The morphology
25 profiles of YFP/CFP positive aggregates were assessed from stack images (50 ± 10 aggregates
26 per condition).

27

28 **RESULTS**

29 In addition to the six 17q21.31 duplication carriers already reported by our group [15, 21], and
30 the two reported in the Chen et al. paper [4], we have identified two unrelated novel cases
31 carrying the same rearrangement, leading to a total of 10 cases from 9 families. In all cases, the
32 size of the duplicated segment was identical and encompassed the entire *MAPT* coding
33 sequence. As displayed in Table 1, these microduplications occurred in different H1/H2
34 haplotypic backgrounds.

1
2
3
4
5
6
7
8
9
10
11
12
13
14
15
16
17
18
19
20
21
22
23
24
25
26
27
28
29
30
31
32
33
34

Clinical features

Clinical phenotypes of all 10 carriers are summarized in Table 1. Mean age of onset was 51.3 years (range: [37-57]) with 6/10 being male patients. In 8 cases, an amnesic syndrome was the main clinical phenotype. Among them, 4 patients initially showed exclusive memory impairment, 3 presented with memory loss associated with either apathy or other behavioral disturbances and one first exhibited behavioral disorder and then memory impairment. The cognitive follow-up of seven patients including a verbal episodic memory assessment by the Free and Cued Selective Reminding Test, revealed a hippocampal dysfunction defined as an abnormal free recall without normalization of the cued retrieval [23]. On the remaining cognitive domains, behavioral and cognitive dysexecutive syndromes (following criteria available at ref. [10]) were identified for 6 patients. Accordingly, the verbal fluency was in abnormal ranges in all of them. None of them presented with visuoperceptual impairment. Neurological examination of these 8 patients was otherwise unremarkable at first visit. In particular, there was not any motor, sensitive, pyramidal tract or extrapyramidal signs. No vertical gaze palsy was noticed. All of them gradually declined towards a severe memory deficit with misorientation and gesture apraxia inducing a progressive impact on instrumental activities of their daily living.

Both cases with an initial akinetic-rigid syndrome developed gait disorders with falls associated with dysarthria, resting tremor and genito-urinary dysfunction. Symptoms were considered levodopa moderately sensitive in EXT_2000_001 and levodopa-resistant in EXT_1998_001. No vertical gaze palsy was reported for EXT_1998_001; it was noted only during the last year before death of EXT_2000_001. In this last patient, executive and attention deficits with judgment impairment and perseverative ideas were reported after a time course of five years (one year before death). Unfortunately, no detailed cognitive assessment was available for this patient. In patient EXT_1998_001, a memory impairment was present at first examination and progressively worsened, 4 years after onset of motor signs and 3 years before death (MMSE scored 23/30 at year 4 and MMSE scored 17/30 with complete temporal disorientation at year 5). Due to these unusual clinical presentations, main clinical hypotheses during the follow-up of both patients were first multiple system atrophy with predominant parkinsonism and then atypical progressive supranuclear palsy (PSP).

Among this group of *MAPT* duplication carriers, at the present time, five patients have died from their disease. Autopsies were available in 4 of them. Mean disease duration was 10.1 years [5-20] when considering the whole group of carriers and 12.0 years when restricting to deceased

1 patients.

2

3 **CSF biomarkers**

4 As can be seen in Table 1, CSF tau and p-tau values were in the abnormal ranges while CSF A β
5 was normal in the two novel patients (EXT_1593_001 and EXT_1687_001). In one previously
6 reported individual (ALZ_596_001) with an A β ₄₂ value below the threshold, a second CSF
7 biomarker assessment following a novel lumbar puncture (4 years after the first one) showed
8 an A β ₄₂ value in the normal range (646 pg/mL). Overall, CSF A β ₄₂ values were considered in
9 the normal ranges in 4/6 patients tested.

10

11 **Brain imaging patterns (MRI, FDG-PET, DAT-SCAN)**

12 MRI scans, performed between one and five years after disease onset, were available for eight
13 patients. White matter hyperintensities on FLAIR-weighted images were present in 3/8 patients
14 but were mild, punctiform and periventricular for ALZ_596_001 and EXT_1114_001 (with a
15 medical history of vascular risk factors) or posterior, moderate and periventricular for
16 EXT_1593_001 (who presented smoking addiction) (Fig. 1a). Cortical atrophy was present in
17 all patients although differentially located. Internal temporal atrophy was found in all cognitive
18 patients, associated with anterior temporal atrophy in three patients (ALZ_596_001,
19 EXT_1687_001, ALZ_441_005) or parietal and occipital atrophy in another three
20 (EXT_1593_001, EXT_1114_001 and ROU_1373_001) (Fig. 1a to 1d). Conversely, no cortical
21 atrophy was noticed for patients EXT_1998_001 and EXT_2000_001.

22 Functional imaging using FDG-PET or HMPAO-SPECT, showed a pattern consistent with the
23 atrophy profiles on MRI. Tracer uptake was decreased in the temporal cortex of all five
24 analyzed patients. The uptake was additionally decreased in the parietal regions of three
25 patients: ROU_1373_001 (Fig. 1e), EXT_1593_001 and ALZ_441_005. Interestingly, that last
26 patient also showed a severe frontal right hypometabolism.

27 DaTscans were performed in four patients. Only one of them (EXT_2000_001) presented with
28 an extrapyramidal syndrome. The three other patients had no extrapyramidal syndrome, neither
29 at first visit, nor at follow up. Strikingly, all four patients showed significantly decreased uptake
30 of the tracer, suggesting bilateral nigro-striatal dopaminergic neuronal loss, either symmetrical
31 for ROU_1373_001 and EXT_2000_001, or asymmetrical for EXT_1593_001 and
32 EXT_1687_001 (left predominance for both).

33

34 **Molecular imaging**

1 Amyloid PET was available in three patients (already reported in [15]) including in patient
2 ALZ_596_001 with initially low and then normal CSF A β ₄₂ values, and in patient
3 EXT_1114_001 with abnormal A β ₄₂ values. Amyloid PET scans were all considered as normal
4 (Table 1).

5 Tau-PET imaging using [¹⁸F]-flortaucipir was performed in two patients. On visual inspection,
6 we found that the tracer binding, eight years after disease onset, was strongly increased in the
7 temporal lobes and in the posterior and superior region of the frontal lobes of ALZ_596_001
8 (Fig. 1f). The other patient (ROU_1373_001) had less pronounced [¹⁸F]-flortaucipir binding on
9 the imaging performed nine years after onset. The uptake was restricted to the medial and
10 anterior temporal regions. A control group of 13 individuals was used to calculate the mean and
11 the standard deviation (SD) of the SUVRs in the regions of interest. The SUVRs of ALZ
12 596_001 were above mean plus 1.96 SD of controls (95% confidence interval), in the temporal
13 lobes (parahippocampal, fusiform, inferior temporal and temporo-polar regions), as well as in
14 the supplementary motor areas. In patient ROU 1373_001, only the parahippocampal gyri and
15 right temporal pole were above mean plus 1.96 SD (Fig. 1g).

16

17 **Neuropathological findings**

18 Neuropathological findings are summarized in Fig. 2, Fig. 3, Table 2, supplementary Fig. 1,
19 supplementary Fig. 2, supplementary Fig. 3, Table 2 and supplementary Table 1.

20

21 **ALZ_441_005**

22 At autopsy, the brain was extremely atrophic, the left hemisphere weighted 347 g after formalin
23 fixation. Macroscopic examination of the left hemisphere revealed a severe atrophy of the
24 frontal, temporal and parietal lobes, mostly affecting the association cortices. The striatum was
25 also atrophic, in particular the caudate nucleus. The hippocampus and amygdala were barely
26 identifiable (Supplementary Fig. 1a, b). The brainstem also showed a generalized atrophy. There
27 was a loss of pigment of the *substantia nigra* and the *locus caeruleus* was not identifiable.
28 Finally, in the cerebellum, in addition to a chronic cavitory infarction of the left hemisphere,
29 there was an atrophy of the dentate nucleus.

30 Histology revealed massive neuronal loss, severe astrogliosis and marked spongiosis in the
31 regions where atrophy was seen at macroscopic examination. These neurodegenerative changes
32 were associated with severe degeneration of the adjacent subcortical white matter.

33 Immunohistochemistry using the AT8 anti-tau antibody revealed a great number of
34 hyperphosphorylated tau deposits in neurons, astrocytes and less frequently in oligodendrocytes

1 as well as in the neuropil. Tau positive aggregates were numerous and seen predominantly in
2 the neocortex, striatum, pallidum, limbic regions, including the hippocampus and entorhinal
3 cortex (Fig. 2a, b, Fig. 3) and the cerebellum. Neocortical pathology involved the frontal,
4 temporal and parietal lobes with very little tau pathology in the occipital cortex. Tau pathology
5 predominated in the grey matter and was scant to moderate in the white matter. In the
6 brainstem, AT8-positive aggregates were numerous in the midbrain and the pons but not in the
7 medulla oblongata. In neurons, the majority of the deposits were spherical inclusions
8 reminiscent of Pick bodies (Fig. 2a). Although the aggregates were mainly 3R-tau, a significant
9 number of inclusions were also 4R-tau immunoreactive. They did not show argyrophilic
10 properties with the Bielschowsky silver staining, except for a few neurons in the dentate gyrus
11 and CA1 regions of the hippocampus, but were positive for Gallyas silver staining (suppl table
12 1). Neurons with diffuse cytoplasmic neuronal immunoreactivity or globose neurofibrillary
13 tangles (NFTs) were also observed but in a much lesser number. In the dentate nucleus of the
14 cerebellum, coarse grain intracytoplasmic neuronal inclusions predominated (Supplementary
15 Fig. 2). The astrocytic deposits reminded of ramified astrocytes as in Pick's disease (Fig. 2a).
16 They showed tau positivity close to the nucleus and lacked fine prolongations in the astrocytic
17 processes. Of note was the predominance of neuronal intracytoplasmic spherical inclusions and
18 neuropil threads (NTs) with very few glial lesions seen in the striatum (Fig. 2b). Aggregates in
19 oligodendrocytes were not numerous and they were predominant in the white matter of affected
20 regions. Small round spherical inclusions, smaller than the nuclei, similar to those seen in Pick
21 disease, were more abundant than coiled bodies (Supplementary Fig. 2 and 3).
22 Tau aggregates in neurons and astrocytes were labeled with 3R-tau and 4R-tau whereas
23 oligodendrocytes were labelled with 3R-tau and less frequently with 4R-tau. As can be seen in
24 Table 2 summarizing the presence of 3R and 4R-tau deposits among nine brain regions in each
25 available autopsy case, there was a predominance of 3R-tau isoforms over 4R isoforms in
26 neurons and astrocytes of all examined brain regions. It is noteworthy that the striatal neuronal
27 deposits were strictly labeled by 3R but not 4R-tau (Fig. 2b). Neuronal, astroglial and
28 oligodendrocytic aggregates were immunoreactive for p62 and AT100. Argentophilic properties
29 were variable depending on the region. A few neuronal globular deposits showed argentophilia
30 with Bielschowsky staining in the dentate gyrus of the hippocampus while they were negative
31 for Gallyas, as seen in Pick disease (Supplementary Fig. 3c). However, in the frontal cortex and
32 striatum they were positive for Gallyas and negative for Bielschowsky silver staining. Small
33 globular oligodendroglial deposits in the white matter showed argyrophilic properties both with
34 the Gallyas and Bielschowsky stainings (Supplementary Fig. 3b).

1 Sarkosyl-insoluble fractions from the frontal cortex and striatum blotted with phospho-tau
2 antibody revealed two main bands at 55 and 64 kDa, similar to the pattern observed in a PiD
3 case processed in parallel. Consistently, when blotted with a 3R-tau antibody, these western
4 blots showed intense immunoreactivity whereas no immunoreactivity was detected with the
5 4R-tau specific antibody (Fig. 4a).

6 Overall, the morphology of tau aggregates was reminiscent of that observed in PiD. However,
7 immunohistochemical and argyrophilic properties of the aggregates showed some differences
8 and there was abundant pathology in the dentate nucleus of the cerebellum, which is not usually
9 observed in PiD. Furthermore, white matter pathology was scant and the globular
10 oligodendroglial aggregates were of small size compared to the ones seen in globular glial
11 tauopathy.

12

13 **ALZ_596_006**

14 The fixed left hemisphere weighted 587 g. Macroscopic examination revealed a moderate
15 atrophy of the medial region of the temporal lobe associated to a moderate ventricular dilatation
16 (Supplementary Fig. 1c).

17 Histology showed marked neuronal loss associated with reactive gliosis in the amygdala, the
18 hippocampus and the entorhinal cortex. A mild to moderate neuronal loss was seen in the
19 nucleus basalis of Meynert, the *substantia nigra* and the *locus caeruleus*. The cerebellum
20 appeared intact at hematoxylin and eosin (H&E) examination.

21 Immunohistochemistry revealed marked tau pathology in the neocortex where there was a
22 predominance of tau positive astrocytes, with moderate number of NFTs and NTs (Fig. 2a). Tau
23 deposits in the astrocytes had various morphologies: some accumulated tau near the nucleus,
24 others had fine deposits in the distal part of the processes and in others the deposits were seen
25 along the length of the processes. In the striatum, the number of tau aggregates was moderate
26 and involved the neurons with the presence of many NFTs and NTs (Fig. 2b). Very few tau
27 positive astrocytes were seen in the striatum (Fig. 3). Tau pathology in the pallidum was rare
28 (Supplementary Fig. 2). In the brainstem, tau pathology was abundant in the *substantia nigra*,
29 which showed many globose NFTs and NTs (Supplementary Fig. 2). In the pons, tau deposits
30 were observed mainly in the tegmentum, including the *locus caeruleus*. Both neuronal and
31 astrocytic deposits were seen. In the medulla oblongata, tau pathology predominated in the
32 reticular formation. The cerebellum had very few aggregates in the dentate nucleus
33 (Supplementary Fig. 2). Oligodendrocytes were only observed in the reticular formation of the
34 medulla and the amygdala. Subependymal, perivascular and subpial thorny astrocytes were

1 seen in the medial region of the temporal lobe and striatum suggesting the presence of
2 associated aging-related tau astroglialopathy (ARTAG) (Supplementary figure 3). A few clusters
3 of astrocytes in the white matter of the frontal, parietal and occipital lobe were also seen. Tau
4 pathology in the medial temporal lobe with numerous NFTs and NTs in the hippocampus, the
5 entorhinal cortex and the amygdala were also observed (Supplementary figure 3). Occasional
6 diffuse A β plaques were seen in the cortex. All of the deposits were positive for p62 and AT100.
7 Neuronal aggregates were immunoreactive for 3R-tau and 4R-tau. In contrast, astrocytes were
8 only 4R-tau positive. Silver staining was variable. Neurons and astrocytes were positive for
9 Gallyas silver staining and only occasional neuronal aggregates and rarely astrocytes were
10 argyrophilic with Bielschowsky (suppl figure 3). As can be seen in Table 2 and Fig. 2, when
11 analyzed for tau isoforms, neuronal aggregates were 3R- and 4R-tau positive with a
12 predominant 3R labelling in almost all structures examined. As in case ALZ_441_005 the
13 striatum was only immunoreactive for 3R-tau. Western blot of insoluble fractions from frontal
14 cortex and striatum, labeled with AT270 antibody showed three bands similar to those seen in
15 AD. The two lower bands were intensively labelled by 3R-tau while the upper and middle bands
16 were labelled by 4R-tau (Fig. 4b).

17 Overall, this case shows a tauopathy (3R>4R) that mainly involves neurons and astrocytes, in
18 cortical and subcortical regions, in which tau aggregates adopt diverse morphologies.
19 Distribution and biochemical properties of the lesions did not fulfill the criteria for either of the
20 known tauopathies.

21

22 **EXT_1998_001**

23 The right hemisphere fixed in formalin weighed 391g (brainstem and cerebellum not included).
24 Gross examination of the coronal sections did not show atrophy of the brain parenchyma
25 (Supplementary Fig. 1d). The study of the mesencephalon was limited, as the brainstem had
26 been previously separated from the hemisphere through this region. However, the rest of the
27 brainstem appeared to have a normal size at macroscopic examination. The *locus caeruleus* was
28 not identified.

29 Histology showed, in addition to widespread anoxic lesions, a tauopathy involving the
30 brainstem, pallidum, striatum, thalamus and dentate nucleus of the cerebellum. In the brainstem,
31 the pallidum and the dentate nucleus, the most prominent AT8 positive tau inclusions were
32 globular bodies, diffuse neuronal intracytoplasmic granular immunoreactivity and NTs
33 (Supplementary Fig. 2). Coiled bodies were seen in the pallidum. Tufted astrocytes were the
34 only tau pathology seen in the striatum (Fig. 2b). In the frontal cortex, the pathology was limited

1 but the extensive laminar necrosis and massive neuronal loss could have explained the scarcity
2 of tau deposits which were predominantly found in tufted astrocytes (Fig. 2a). A few NTs and
3 coiled bodies in the subjacent white matter were seen. In the medial and lateral regions of the
4 temporal lobe, tau pathology which included NFTs, granular intracytoplasmic aggregates, NTs
5 and ghost tangles was severe. Immunohistochemistry for tau antibodies in the frontal cortex
6 and striatum revealed that tau pathology was only of the 4R isoforms, while 3R-tau
7 immunohistochemistry was negative (Fig. 2). Neuronal and astrocytic aggregates were
8 immunoreactive for p62 and AT100. Oligodendrocytes showed frequent immunoreactivity for
9 AT100 but it was rare for p62. Silver staining showed positivity for Gallyas while Bielschowsky
10 was negative (Supplementary Table 1). In medial temporal brain regions, the deposits,
11 consistent with Braak stage II-III tau pathology, were labeled with both 3R and 4R-tau (Table
12 2).

13 Sarkosyl-insoluble fraction from the frontal cortex and striatum blotted with AT270 antibody
14 showed a two-band profile reminiscent of PSP. When blotted with a 3R-tau antibody, samples
15 from frontal cortex did not show any immunoreactivity, while samples extracted from the
16 striatum showed a faint, 2-band pattern, corresponding to 55 and 64kDa Tau bands. Both
17 samples were labeled by the 4R-tau antibody, with a similar pattern to that seen with the AT270
18 antibody, confirming that tau aggregated, in these regions, was mainly 4R (Fig. 4c).

19

20 **EXT_2000_001**

21 The formalin fixed whole brain weighted 1200 g. At gross examination, the *substantia nigra*
22 was pale and the subthalamic nucleus, atrophic. There was a moderate dilation of the 3rd
23 ventricle (Supplementary Fig. 1e). Histologic examination with hematoxylin-eosin (H-E)
24 evidenced, in accordance with the macroscopic observations, a massive neuronal loss in the
25 *substantia nigra*. The neuronal loss was severe in the subthalamic nucleus. The pallidum was
26 gliotic. The neocortex and the hippocampus appeared normal.

27 Tau positive aggregates were mainly detected in subcortical regions (especially in the basal
28 ganglia and in the brainstem) and were minimal in the frontal cortex and hippocampus (Fig. 2a,
29 b; Supplementary Fig. 1). The predominant lesions were NFTs, sometimes globose, NTs and
30 astrocytic deposits. In the astrocytes, AT8 tau positive aggregates were atypical, close to the
31 nuclei with little ramifications. In the caudate nucleus, however, the morphology of the
32 astrocytic aggregates was similar to that of tufted astrocytes (Fig. 2a, b). Coiled bodies in the
33 oligodendrocytes were infrequent. In the striatum, aggregates were seen in the caudate nucleus
34 while they were scarce in the putamen. The internal capsule was the only region that showed

1 many coiled bodies and NTs were also frequent. Tau pathology was marked in the pallidum
2 (Supplementary Fig. 2). While the thalamus was moderately involved the subthalamic nucleus
3 had massive pathology with a predominance of neuronal deposits (NFTs and NTs). Mainly
4 globose NFTs were seen in the nucleus basalis of Meynert. In the brainstem there was a large
5 number of deposits in the *substantia nigra* and the periaqueductal grey of the mesencephalon.
6 In the pons, tau aggregates were numerous in the tegmentum while they were rare in the ventral
7 pons (Supplementary Fig. 2). In the medulla oblongata, the aggregates predominated in the
8 reticular formation, in the cranial nerve nuclei and in the inferior olive, where mainly NFTs
9 were seen. In the cerebellum the presence of many coarsened granular neuronal intracytoplasmic
10 aggregates and NTs in the dentate nucleus was surprising compared to its normal appearance
11 after H-E staining. All of the tau deposits seen were positive for the 4R isoforms and negative
12 for the 3R isoforms (Table 2, Fig. 2). In the entorhinal cortex tau aggregates expressed both 3R
13 and 4R isoforms, consistent with Braak stage II tau pathology. As with the previous case, all of
14 the tau aggregates were positive for AT100. P62 immunoreactivity was also seen in all types
15 of aggregates, however it was scant compared to the amount of tau pathology seen. Similarly
16 to the previous case, tau aggregates were positive for Gallyas and negative for Bielschowsky
17 silver staining. No Western blot analysis was undertaken due to the lack of frozen tissue.
18 Overall, the distribution and characteristics of tau pathology in cases EXT_1998_001 and
19 EXT_2000_001 was reminiscent of that observed in progressive supranuclear palsy (PSP)
20 cases. However, compared to sporadic PSP, in our two cases, oligodendrocytes with tau
21 pathology (coiled bodies) were scant and tau aggregates in the pontine basis were rare.

22

23 **No evidence for associated proteinopathies**

24 There was no associated α -synuclein or TDP-43 proteinopathies in any of the cases
25 (Supplementary Fig. 7). No A β deposits were observed except in case ALZ_596_006 where
26 rare diffuse A β plaques were seen in the cortex of the middle frontal gyrus, the subcallosal area
27 and the inferior temporal gyrus. No A β oligomers were detected by western blot analysis of
28 the frontal cortex of the three cases with available frozen tissue (Supplementary Fig. 4)

29

30 **Analysis of exon 10 splicing and determination of 4R/3R tau mRNA ratios**

31 The alternative splicing of exon 10 in mature *MAPT* mRNA naturally leads to either 3R-tau (in
32 case of exon 10 skipping) or 4R-tau (in case of exon 10 inclusion). In an attempt to identify
33 genetic variants influencing alternative splicing of exon 10, we sequenced exon 10 boundaries
34 in the nine cases with available DNA. No single nucleotide variant, short insertion or deletion

1 putatively influencing splicing was found.
2 *MAPT* 4R/3R mRNA ratios were analyzed in two cerebral regions (frontal cortex and striatum)
3 for the three patients for whom frozen tissue was available (EXT_1998_001, ALZ_596_006
4 and ALZ_441_005) and for five normal controls. In controls, the 4R/3R mean ratio was $0.69 \pm$
5 0.10 (SEM) in the frontal cortex and 0.97 ± 0.16 (SEM) in the striatum. For each control, the
6 4R/3R ratio was systematically increased in the frontal cortex compared to striatum, but this
7 increase was collectively not significant ($p=0.125$, Wilcoxon signed ranked test). In the frontal
8 cortex of the patient with 3R-tau aggregates resembling Pick bodies (ALZ_441_005), we noted
9 a 243% increase of the 4R/3R mRNA ratio as compared to the mean value in controls, which
10 is in the same range as published data in patients with Pick disease [13]. In the striatum, 4R/3R
11 mRNA ratios were higher in both patients with mainly 3R-tau aggregates (ALZ_441_005 and
12 ALZ_596_006) (136% and 139 % increase, respectively) and lower (74%) for the patient with
13 mainly 4R-tau aggregates (EXT_1998_001) as compared with the controls mean value
14 (Supplementary Fig. 5).

15

16 **In vitro seeding experiments**

17 All homogenates derived from samples containing misfolded tau induced the aggregation of
18 the endogenous tau RD P301S proteins expressed by the biosensor (Fig. 5; Supplementary Fig.
19 6). The intracellular aggregates of tau proteins observed in biosensor cells was of different
20 types: some aggregates were granular (types 1 and 2), while others appeared larger and denser
21 (types 3 and 4; Fig. 5a). Morphological features of induced aggregates of three *MAPT*
22 duplication carriers (ALZ_441_005, ALZ_596_006 and EXT_1998_001) showed
23 dense/granular ratios between those induced by homogenates of a PiD and a PSP control (Fig
24 5b), at both extremes. Indeed, the seeding-competent homogenates derived from ALZ_441_005
25 and PiD cases led to a majority of granular aggregates of tau proteins, that represented
26 respectively 66.44% [95%CI: 58.86;74.02] and 67.35% [95%CI: 59.77;74.93] of total
27 aggregates (Z-test comparison to the null hypothesis of equal proportions: $p < 0.0001$ for ALZ
28 441_005 and PiD cases, as shown in Fig. 5b). Interestingly, dense/granular ratios did not differ
29 significantly between ALZ_441_005 and the PiD case (Fig 5c). Conversely, samples obtained
30 from EXT_1998_001 and PSP cases both induced a majority of dense aggregates, reaching a
31 proportion of 63.83% [95%CI: 55.90;71.76] and 76.97% [95%CI: 70.28;83.67], Z-test
32 comparison to the null hypothesis of equal proportions: $p=0.0014$ for EXT_1998_001 case and
33 $p < 0.0001$ for PSP case, as shown in Fig. 5b). Finally, the samples obtained from ALZ_596_006

1 showed an intermediate proportion of dense/granular aggregates (proportion of dense
2 aggregates: 56.21% [95%CI: 48.73;63.69]; Z-test comparison to the null hypothesis of equal
3 proportions: $p=0.1239$).

4

5 **DISCUSSION**

6 The biological, imaging and neuropathological data presented here definitely settle one issue:
7 the 17q21.31 duplication causes a primary tauopathy showing various combinations of well-
8 characterized primary tauopathies, and not an atypical form of AD. Previous CSF biomarker
9 data suggesting an A β pathology in 3/4 *MAPT* duplication carriers were not supported by a
10 reassessment in one patient and more recent data obtained in two additional patients in whom
11 A β levels were in the normal range. Furthermore, all three amyloid PET scans were negative;
12 there were no senile plaques at neuropathological examination and minimal A β staining was
13 present in only one case. We further ensured that no A β oligomers were detected, ruling out any
14 involvement of this peptide in the pathology. Of note, the case reported by Alexander et al. [1]
15 showed asymmetric TDP-43 deposits. We hypothesize that it could be co-incidental in this case,
16 as none of our patients showed such immuno-reactivity, even though only one hemisphere was
17 examined in all four cases.

18 Clinically, we identified eight patients presenting with episodic memory impairment following
19 a profile observed in typical AD [8] with or without behavioral symptoms upon presentation,
20 on one side, and one patient with an isolated atypical extrapyramidal presentation resembling
21 the one observed in progressive supranuclear palsy (PSP), on the other side. These clinical
22 presentations appear as two extremes, belonging to a spectrum. That hypothesis is supported
23 by (i) the association, in the remaining case with an atypical extrapyramidal syndrome upon
24 presentation, of an early memory impairment that worsened during follow up and (ii) the fact
25 that three cases with memory impairment upon presentation also exhibited significant
26 dopaminergic nigrostriatal neuronal depletion as observed on DaTscan imaging despite normal
27 physical examination, thus suggesting partial alteration of dopaminergic pathways however
28 insufficient to induce the emergence of extrapyramidal signs as described in premotor
29 Parkinson's disease stages [25]. Interestingly, in the family described by Alexander et al.[1],
30 both the proband and his sister presented memory and behavioral impairment, with
31 neuropsychological assessments and MRI consistent with a diagnosis of probable AD, but also
32 exhibited mild to moderate extrapyramidal symptoms upon examination.

33 Neuropathological examination combining immuno-histochemical and biochemical analyses
34 supports such a continuum by showing that different tau isoforms formed aggregates among

1 the four examined brains. In one case with a cognitive and behavioral disorder presentation
2 (ALZ_441_005), we observed widespread tau deposits in the hippocampus and neocortex,
3 which were mainly composed of 3R-tau as in Pick disease although globular inclusions were
4 Gallyas positive and Bielschowsky negative in the striatum and frontal cortex. Thus, this case
5 harbors a novel variety of Pick body-like inclusions in addition to those already associated with
6 some *MAPT* pathogenic variants [2, 19, 26]. In contrast, in the case presenting with isolated
7 atypical extrapyramidal syndrome (EXT_2000_001), the picture was reversed: we observed tau
8 aggregates mainly located in subcortical regions, which were exclusively composed of 4R-tau
9 protein isoforms. Those two cases may be seen as the extremes of the spectrum: between those
10 two extremes, patient EXT_1998_001, who exhibited an akinetic-rigid syndrome associated
11 with a severe memory deficit, showed a mixed 3R/4R tauopathy, albeit with 4R-tau
12 predominant deposits in the striatum and frontal cortex. The clinical picture, the 4R-tau
13 predominance, the presence of 3R-tau accumulation in the subcortical nuclei is reminiscent of
14 the case published by Alexander et al. [1]. In the last case (ALZ_596_006), closer to the
15 dementia side, a mixed 3R/4R tauopathy similar to that seen in AD was found with severe
16 involvement of the medial region of the temporal lobe.

17 Overall, *MAPT* duplication can thus lead to a spectrum of primary tauopathies with 3R- or 4R-
18 tau predominant aggregates. Our observations suggest that 4R-tau deposits involve together
19 basal nuclei, brainstem and basal ganglia, and are associated with motor symptoms. On the
20 other hand, 3R-tau predominant cortical inclusions were associated with Pick-like inclusions.
21 Those conclusions, based on the analysis of a small number of cases, obviously await
22 confirmation by further studies.

23 Of note, *in vivo* tau PET imaging could reflect neuropathological heterogeneity of the tau
24 pathology. Postmortem studies showed that the affinity of the tau tracer for non-AD tau lesions
25 may be lower than that for AD tauopathy, with low or absent binding of [¹⁸F]-Flortaucipir to
26 tau straight filaments [17]. The distinct tau PET binding profiles between ALZ_596_006, and
27 ROU_1373_001 could reflect a qualitative rather than a quantitative difference of the tau
28 pathology, with a possible different mixed 3R/4R tauopathy in ALZ_596_001, whose tau tracer
29 uptake was clearly increased in the temporal lobes. The tau tracer binding was far less
30 pronounced in ROU_1373_001, who had nevertheless a similar clinical presentation, disease
31 duration, and FDG-PET pattern. This could reflect a different type of tau lesions for which the
32 tracer has less affinity.

33 We sought to identify a putative correlation between the preferential accumulation of 4R- or
34 3R-tau and the relative expression of tau transcripts. Focusing on the striatum where either 4R

1 or 3R-predominant tau aggregates were present in patients, we failed to find a positive
2 correlation with 4R/3R mRNA ratios. Rather, the relative proportion of 4R-containing
3 transcripts was moderately increased in patients ALZ_441_005 and ALZ_596_006 with 3R-tau
4 aggregates whereas the converse was observed in patient EXT_1998_001 with 4R deposits.
5 Consistent with previous findings in PSP and PiD patients [13], the preferential accumulation
6 of 4R- or 3R- tau aggregates is neither driven by the corresponding preferential expression of
7 the 4R or 3R-encoding transcripts, nor by the *MAPT* haplotype associated with the duplication.
8 It has been suggested, although this claim remains controversial [28], that the *MAPT* H1
9 haplotype [3] or sub-haplotypes [18], is associated with increased expression of 4R tau-
10 encoding transcripts. Accumulation of 3R-tau in ALZ_441_005 occurred in the 2H1-1H2
11 background whereas accumulation of 4R-tau in EXT_1998_001 occurred in the 1H1-2H2
12 background: only one H1 haplotype was thus present in a case with 4R-tau predominant
13 accumulation while they were two in a case in which 3R-tau was the preferential isoform, in
14 contradiction with the hypothetical role of the H1 haplotype. Finally, the search of rare or
15 common variants in exon 10 and surrounding splicing regions, which could have influenced the
16 3R/4R tau mRNA ratios remained negative. We conclude that the shift toward 3R or 4R-tau
17 predominant pathology and the topography of lesions do not appear to be directly related to a
18 change in the balance between the corresponding transcripts.

19 Local factors influencing availability or aggregation properties of different tau isoforms might
20 explain why, in the general context of tau overexpression, aggregates are preferentially formed
21 of 3R- or 4R-tau in discrete brain regions of a same individual. The striking inter-individual
22 differences in the composition of aggregates observed in identical brain regions suggest,
23 however, that this process could also be driven by the formation of different pathogenic seeds:
24 peculiar sets of 3R or 4R misfolded tau proteins could aggregate in specific parts of the brain
25 and subsequently spread in other cerebral regions along anatomically connected networks [5].
26 Tau pathology located in the striatum of ALZ_441_005, ALZ_596_006 and EXT_1998_001
27 cases induced different types of tau aggregates in a biosensor cell line expressing tau RD P301S
28 (4R-tau): the striatum of ALZ_441_005 containing 3R-tau inclusions mainly led to granular
29 aggregates (similarly to a PiD homogenate), whereas the striatum of EXT_1998_001 presenting
30 4R-tau inclusions mostly resulted in dense aggregates (as observed with a PSP homogenate).
31 The striatum of ALZ_596_006, containing a mixture of 3R- and 4R-tau lesions, seeded the
32 formation of granular and dense aggregates in similar proportions. Those morphological
33 features were independent of the sample seeding potential, as tau seeding activity appeared
34 higher in ALZ_441_005 and PSP homogenates than in EXT_1998_001 and PiD samples, after

1 a total tau normalization (Supplementary Fig. 6). Our results thus support the hypothesis of
2 different seeds among *MAPT* duplication cases. In the context of moderate *MAPT*
3 overexpression related to the duplication, tau monomers could adopt different abnormal
4 conformations leading to several seed competent species. Depending on the “strains”, mainly
5 3R or 4R-tau could be preferentially incorporated, leading to various protein assemblies,
6 resulting ultimately in different pathologies characterized by fibril morphology, cellular type
7 specificity and anatomical spreading patterns. Also supporting this hypothesis, it has recently
8 been shown that stochastic misfolding of tau conformers occurs in brain tissues of patients
9 carrying the same P301L *MAPT* mutation, followed by templated conversion of native
10 monomers [7].

11 In summary, we have identified different types of *MAPT* duplication carriers exhibiting, at least
12 in early stages of their diseases, different cognitive or motor symptoms related either to cortical
13 or subcortical dysfunctions and characterized by the accumulation of different tau isoforms.
14 Given the diversity of clinical and imaging presentations and the simplicity of the genetic test,
15 we suggest searching *MAPT* duplications in all cases with early-onset idiopathic
16 neurodegenerative dementia or early-onset idiopathic atypical extrapyramidal syndromes. They
17 should also be sought when neuropathologically-identified primary tauopathies are not related
18 to *MAPT* mutations, particularly when the unusual constellation of tau pathology cannot be
19 clearly put in one of the boxes of currently described primary tauopathies.

20

1 **FIGURE LEGENDS**

2 **Figure 1. Structural, functional and Tau PET Cerebral imaging of MAPT duplication**
3 **carriers**

4 a. FLAIR-weighted axial MRI scan of EXT_1593_001 showing parietal cortical atrophy and
5 mild white matter hyperintensities

6 b. T1-weighted coronal MRI scan of EXT_1114_001

7 c. T1-weighted coronal MRI scan of ROU_1373_001

8 d. FLAIR-weighted sequence coronal MRI scan of EXT_1687_001

9 e. FDG-PET scan of ROU_1373_001 showing parietal bilateral hypometabolism (arrows)

10 f. Tau-PET imaging of ALZ_596_001 with color scale corresponding to the SUVR scale

11 g. Tau-PET imaging of ROU_1373_001 with color scale corresponding to the SUVR scale

12

13 **Figure 2. Tau pathology of the four cases carrying an *MAPT* duplication in the frontal**
14 **cerebral cortex (A) and the caudate nucleus (B).**

15 **a. Diversity of tau pathology and 3R- and 4R-tau isoform expression in the frontal cortex.**

16 In ALZ_441_005, pathology was abundant with a predominance of neuronal deposits with
17 many globular Pick-like bodies in the neurons. Astrocytic deposits were also numerous and
18 reminded of tufted astrocytes with deposits close to the nucleus and without the ramifications.

19 In ALZ_596_006, there was a predominance of astrocytic pathology with many tufted
20 astrocytes and some neurofibrillary tangles (NFTs) in neurons. Tau pathology in
21 EXT_1998_001 and EXT_2000_001 was scant and only a few deposits in the form of tufted
22 astrocytes and a few NFTs in neurons were seen. Tau aggregates in ALZ_441_005 and
23 ALZ_596_006 included the 3R- and 4R-tau isoforms. EXT_1998_001 and EXT_2000_001 tau
24 aggregates expressed solely 4R-tau. *Frontal cortex. Immunohistochemistry: AT8, 3R-tau, 4R-*
25 *tau. Scale bar in first row 100µm, Scale bar in four last rows 25µm.*

26 **b. Diversity of tau pathology and 3R- and 4R-tau isoform expression in the caudate**

27 **nucleus.** In ALZ_441_005, pathology was abundant with a predominance of neuronal
28 pathology with many globular Pick-like bodies in neuronal soma and abundant neuropil threads.

29 In ALZ_596_006 neuropil threads were many, however neuronal neurofibrillary tangles (NFT)
30 were moderate in number. In EXT_1998_001 and EXT_2000_001, pathology was
31 predominantly astroglial with astrocytic deposits resembling tufted astrocytes. ALZ_441_005
32 and ALZ_596_006 expressed only 3R-tau isoforms and EXT_1998_001 and EXT_2000_001
33 were positive only for 4R-tau immunohistochemistry. *Caudate nucleus.*
34 *Immunohistochemistry: AT8, 3R-tau, 4R-tau. Scale bar in first row 100µm, Scale bar in last*

1 *three rows 25 μ m.*

2

3 **Figure 3. Distribution and intensity of tau pathology in the brain of *MAPT* duplication**
 4 **carriers.**

5 Color-coded table following a quantitative evaluation of tau pathology by regions of the brain.
 6 Semiquantification of total tau pathology (**total**) in **neurons, astrocytes, oligodendrocytes** and
 7 neuropil (**neuropil threads**) in relevant brain regions. Blue=0; Green=rare or scant;
 8 Orange=moderate; Red=abundant. NA: not available. (a) Tau pathology is seen in the anterior
 9 part of the putamen in case ALZ_596_006 and EXT_1998_001 (b) Tau pathology only involves
 10 the external pallidum in case ALZ_441_005. ctx: cortex; wm: white matter; CA: cornu
 11 Ammonis; DG: dentate gyrus; Sub: subiculum; Subth: subthalamic nucleus; SN substantia
 12 nigra; PGM: periventricular gray matter; RN: red nucleus; PT: pontine tegmentum; BP: basis
 13 pontis; RT reticular formation; inf olive: inferior olive; dentate: dentate nucleus

14

15 **Figure 4. Western blots of sarkosyl-insoluble 4R and 3R-Tau in patients and controls.**

16 a. Analysis of patient ALZ_441_005 (ALZ 441) ; b. Analysis of patient ALZ_596_006. c.
 17 Analysis of patient EXT_1998_001. For all patients, western blotting was performed on brain
 18 samples extracted from frontal cortex (left panels) or striatum (right panels). Blots were
 19 revealed with antibodies against Tau phosphorylated on Thr181 (AT270 tracks), 3R-Tau (RD3
 20 tracks) or 4R-Tau (RD4 tracks). Tau profiles obtained from the *MAPT* duplication carriers were
 21 compared to those of patients showing Alzheimer's disease (AD), Pick's disease (PiD) or PSP
 22 neuropathology, and to a control individual (Ctrl).

23 Note that western blots are presented here as a composite image from different times of
 24 exposure of a unique blot for each panel (all samples from each panel migrated on a same blot)
 25 to better compare Tau profiles between each antibody despite varying staining intensity.

26 Note that RD4 staining requires longer exposure than using RD3 antibody, so that minor 4R
 27 aggregates as observed in IHC may be hardly detectable in WB performed in similar regions.

28

29 **Figure 5. *In vitro* characterization of tau seeding activity in the striatum of *MAPT***
 30 **duplication cases in a cell biosensor.**

31 HEK cells expressing tau RD P301S coupled with fluorochromes (YFP or CFP) were exposed
 32 to brain homogenates normalized for total tau proteins, obtained from the striatum of a control
 33 case and of three *MAPT* duplication cases, pons of a PSP case and frontal cortex of a PiD case.

34 a. Illustration of the four types of tau aggregates. Type 1: unique and small grain (~ 10% of cell

1 volume or less); Type 2: multiple granules of homogeneous size; Type 3: multiple granules
2 associated with a larger dense core; Type 4: large and dense aggregate (~ 30% of cell volume
3 or more). Representative confocal images with max YFP (yellow), CFP (cyan) and DAPI (blue)
4 intensity projections from a stack covering all the cells contained in the field (scale bar: 10 μ m);
5 no aggregates: example of cells devoid of any aggregates in HEK cells exposed to control brain
6 homogenate, showing diffuse YFP/CFP positive immunofluorescent staining due to non-
7 aggregated tau-RD b. Mean percentages of each type of tau aggregates observed for each case,
8 obtained from three independent experiments in which a total of 50 ± 10 YFP/CFP positive
9 cells were analyzed per condition. Proportions of “granular” (type 1 + type 2) and “dense” types
10 of aggregates (type 3 + type 4) were compared to the null hypothesis of equal proportion using
11 a Z-test for proportions. c. Proportion of cells with dense aggregates. Comparison between two
12 individuals using a Z-test for proportions.

13

14

15

1 **Supplementary Figures**

2 **Supplementary Fig. 1. Morphological variability at macroscopic examination between the**
 3 **four postmortem studied cases:** ALZ_441_005 (A and B), ALZ_595_006 (C),
 4 EXT_1198_001 (D), EXT_2001_001 (E).

5 a. Marked atrophy of the frontal, parietal and temporal association cortices. b. Coronal sections
 6 at two levels, the head of the caudate and the mamillary bodies, showed marked dilatation of
 7 the lateral ventricle, severe atrophy of the striatum (white arrow) and of the temporal lobe (black
 8 arrow). The hippocampus and amygdala are barely identifiable. c.) Moderate atrophy of the
 9 medial temporal lobe (red arrow) associated to a moderate dilatation of the temporal horn of
 10 the lateral ventricle. d and e) Absence of brain atrophy. Moderate dilatation of the 3rd ventricle
 11 in EXT_2000_001 (e). (a and b) left hemisphere; (c) right hemisphere.

12

13 **Supplementary Fig. 2. Diversity of tau pathology in different regions of the brain.** In the
 14 pallidum tau pathology was abundant in all cases except in ALZ_596_006. In the *substantia*
 15 *nigra* tau aggregates were numerous in all cases seen where tissue was available. Globular
 16 tau aggregates in neuronal cell body and neuropil threads were the predominating deposits. In
 17 the pons, the *basis pontis* showed a great number of tau positive aggregates which were globular
 18 in ALZ_441_005. Tau deposits were scant in EXT_2000_001 and were absent in ALZ_596_006
 19 and EXT_1998_001. The dentate nucleus showed abundant coarse granular neuronal
 20 intracytoplasmic aggregates in ALZ_441_005, deposits were moderate in EXT_2000_001 and
 21 scant in the other two cases. The white matter showed little pathology in ALZ_596_006 and
 22 EXT_2000_001 with few neuropil threads. In ALZ_441_005 a moderate number of
 23 oligodendrocytic aggregates were seen and were predominantly globular. In EXT_1998_001
 24 the few oligodendroglial pathology seen adopted a more typical coiled body shape.
 25 Immunohistochemical staining with AT8. *Scale bar in rows 1-4: 50µm, Scale bar in last row:*
 26 *25µm.*

27

28 **Supplementary Fig. 3. a. Immunohistochemical and histochemical characteristics of tau**
 29 **aggregates.** Tau aggregates seen in neurons and astrocytes in the four histological studied cases
 30 (ALZ_441_005, ALZ_596_006, EXT_1998_001, EXT_2000_001) were positive for
 31 phosphorylation dependent AT100 antibody, p62 and Gallyas silver staining. Occasional
 32 neurons and rarely astrocytes in the frontal cortex of case ALZ_596_006 showed argyrophilic
 33 properties with the Bielschowsky silver staining. *Frontal cortex (ALZ_441_005 and*
 34 *ALZ_596_006) and striatum (EXT_1998_001 and EXT_2000_001). Immunohistochemistry:*

1 *AT100 and p62. Silver staining: Gallyas and Bielschowsky. Scale bar 50 μ m except for*
2 *Bielschowsky staining of case ALZ_596_006 which is 25 μ m.*

3 **b. White matter pathology is scant to moderate in ALZ_441_005.** Tau aggregates are seen
4 in some of the oligodendrocytes. There is a predominance of small round aggregates (black
5 arrow) but some coiled bodies are also seen (white arrow head). Tau aggregates express the 3R-
6 tau and 4R-tau isoforms, are AT100 and p62 positive and are argyrophilic with both Gallyas
7 and Bielschowsky silver stains. *Immunohistochemistry: AT8, 3R-tau, 4R-tau, AT100 and p62.*
8 *Silver staining: Gallyas and Bielschowsky. Scale bar for top left image 100 μ m, for top right*
9 *image 50 μ m and for inferior row 25 μ m.*

10 **c. Only rare neurons in the dentate gyrus and CA2 region of the hippocampus are positive**
11 **for Bielschowsky in ALZ_441_005.** *Bielschowsky silver stain. Scale bar: 25 μ m.*

12 **d. Round neuronal intracytoplasmic tau aggregates were observed in the dentate gyrus in**
13 **ALZ_596_006.** The aggregates were immunoreactive for both 3R-tau and 4R-tau antibodies
14 and were positive for Gallyas and Bielschowsky silver staining. *Immunohistochemistry: 3R-tau*
15 *and 4R-tau. Silver stains: Gallyas and Bielschowsky. Scale bar: 25 μ m.*

16 **e. Perivascular thorny astrocytes reminiscent of aging-related tau astroglipathy**
17 **(ARTAG) were seen in the periamygdaloid region.** Additionally, there were occasional
18 astrocytes containing tau aggregates in the subcortical white matter (parietal lobe).
19 *Immunohistochemistry: AT8. Scale bar: 50 μ m.*

20 **f. In case ALZ_596_006, 3R tau and 4R tau neurofibrillary tangles and neuropil threads**
21 **in the hippocampus-CA1.** *Immunohistochemistry: 3R-tau, 4R-tau. Silver staining: Gallyas*
22 *and Bielschowsky. Scale bar: 50 μ m.*

23

24 **Supplementary Fig. 4. Western blot using WO2 antibody** from the frontal cortex of three
25 MAPT duplication carriers, a subject with Alzheimer disease due to an APP duplication a one
26 normal control.

27

28 **Supplementary Fig. 5. Analysis of the 4R/3R ratio of MAPT mRNA.** Extracted from frontal
29 cortex or striatum. The control group (ctrls) consists in the mean of 5 normal individuals. Error
30 bars represent SEM.

31 ALZ 441: ALZ_441_005; ALZ 596: ALZ_596_006, EXT 1998: EXT_1998_001

32

33

1 **Supplementary Fig. 6. Quantitative analysis of tau seeding activity in a cell biosensor.**

2 Proportion of HEK cells containing endogenous tau intracellular aggregates for each tested
3 sample, obtained after 2 x 4 repeated observations in three independent experiments. Patients
4 were compared into a linear mixed effect model for repeated data using Tukey correction for
5 multiple comparisons (Mean of observed proportions \pm SEM: CTRL: 0.22% \pm 0.11%, PiD
6 cortex: 2.90% \pm 0.51%; ALZ_441_005 striatum: 12.22 \pm 0.81; ALZ_596_006: 4.48 \pm 0.61%
7 ; EXT_1998_001 striatum: 5.95% \pm 0.83%; PSP : 14.93% \pm 0.90%). Proportion of cells with
8 aggregates is significantly higher in all patients compared to controls (PiD vs CTRL: p=0.01;
9 other comparison to controls: all p<0.001). Tau seeding activities detected in patients were all
10 pairwise significantly different (ALZ_441_005 vs PSP: p=0.03, EXT_1998_001 vs PiD: p =
11 0.01, all other p<0.001) except for PiD vs ALZ_596_006 (p=0.6) and EXT_1998_001 vs
12 ALZ_596_006 (p=0.6).

13

14 **Supplementary Fig 7. Absence of associated α -synucleinopathy or TDP-43-pathy.**

15 Immunohistochemistry for α -synuclein and TDP-43 was negative in all histological studied
16 cases. A β was negative in three cases (ALZ_441_005, EXT_1998_001, EXT_2000_001). A
17 few diffuse plaques were seen in the neocortex of ALZ_596_006. First column: frontal cortex.
18 Second column: substantia nigra (SN). Third column: dentate gyrus. Scale bar: 50 μ m

19

20 **Supplementary Table 1. Staining properties of tau immunoreactive aggregates in different**
21 **cell types in MAPT duplication carriers.**

22 3R-tau, 4R-tau, AT100 and p62 antibodies. Gallyas and Bielschowsky silver staining. R: tau
23 aggregates are sparsely positive. ND: not determined.

24

25

26

27

| | ALZ_596_001 | ALZ_596_006 | EXT_1593_001 | EXT_1114_001 | ROU_1373_001 | ROU_747_001 | EXT_1687_001 | ALZ_441_005 | EXT_1998_001 | EXT_2000_001 |
|--|--------------------------------|--------------------------------|------------------|------------------|--------------|---------------|--------------|----------------------|----------------------|----------------------|
| Published in / novel case | [15] | [15] | novel | [15] | [15] | [21] | novel | [15] | [4] | [4] |
| Age at onset (years) | 50 | 55 | 56 | 57 | 54 | 49 | 53 | 45 | 57 | 37 |
| Sex | M | M | M | F | M | F | F | M | F | M |
| MAPT haplotype | H1/2H2 | H1/2H2 | H1/2H2 | H1/2H2 | 2H1/H2 | 3H1 | H1/2H2 | 2H1/H2 | H1/2H2 | NA |
| First reported symptoms | memory | memory | memory, behavior | memory, behavior | memory | behavior | memory | behavior, memory | akinetic-rigid synd. | akinetic-rigid synd. |
| Family history of dementia | + (same family as ALZ_596_006) | + (same family as ALZ_596_001) | + | + | - | + | + | - (de novo mutation) | | |
| Extrapyramidal syndrome at onset | - | - | - | - | - | - | - | - | + | + |
| behavioral or cognitive dysexec. synd. | - | | + | + | - | + | - | + | + | + |
| visuoperceptive impairment | - | | - | - | - | | - | - | | |
| Disease duration (years) | 11 | 16 (to death) | 6 | 8 | 10 | 20 (to death) | 6 | 13 (to death) | 6 (to death) | 5 (to death) |
| MRI (years ADO±) | 5 | | 2 | 1 | 4 | | 3 | 2 | 4 | 3 |
| presence of WMH | + | | + | + | - | | - | - | - | - |
| anterior temporal atrophy | + | | - | - | - | | + | + | - | - |
| internal temporal atrophy | + | | + | + | + | | + | + | - | - |

| | | | | | | | | | | |
|-----------------------------------|-------------------|--|--------------|------------|---------------|--|--------------|------------|---|--------------|
| Scheltens score (R/L) | 4-4 | | 3-3 | 3-3 | 3-3 | | 4-3 | 3-3 | | 0-0 |
| frontal atrophy | - | | - | - | - | | - | + | - | - |
| parietal/occipital atrophy | - | | + | + | + | | - | - | - | - |
| HMPAO-SPECT/ FDG-PET (years ADO±) | 3 | | 3 | 3 | 5 | | | 3 | | |
| temporal cortex | P | | P | P | P | | | P | | |
| parietal cortex | N | | P | N | P | | | P | | |
| frontal cortex | N | | N | N | N | | | P | | |
| DaTScan (years ADO±) | | | P (3) | | P (10) | | P (6) | | | P (2) |
| Amyloid-PET (years ADO±) | N (6) | | | N (3) | N (4) | | | | | |
| Tau-PET (years ADO±) | P (8) | | | | P (9) | | | | | |
| CSF Biomarkers (years ADO±) | 3 | | 3 | 3 | 2 | | 2 | 1 | | |
| Aβ42 (pg.mL ⁻¹) | 496 / 646* | | 1372 | 372 | 864 | | 850 | 260 | | |
| Tau (pg.mL ⁻¹) | 558 / 558* | | 789 | 866 | 696 | | 1284 | 507 | | |
| P-Tau (pg.mL ⁻¹) | 66 / 56* | | 82 | 94 | 98 | | 12 | 67 | | |
| Aβ42/Aβ40 | n.a / 0.07* | | 0,16 | | | | 0,06 | | | |

Table 1. Demographic, genetic, clinical, imaging and biological data of all *MAPT* duplication carriers

Cells in grey mean data are not available; +: present; -: absent; dysexec. synd.: dysexecutive syndrome; WMH: white matter hyperintensities; HMPAO-SPECT: hexamethylpropanolamine oxime single photon emission computed tomography; FDG-PET: fluorodeoxyglucose positron emission tomography; ADO±: after disease onset; R: right; L: left; DaTScan: dopamine transporter scan; amyloid-PET: amyloid-tracer positron emission tomography; tau-PET: Flortaucipir tau-tracer positron emission tomography; CSF: cerebrospinal fluid; Aβ: β-amyloid 1-42 peptide; Aβ40: β-amyloid 1-40 peptide; P-Tau: phosphorylated-tau protein; *: novel analysis after second lumbar puncture. Abnormal CSF biomarker values appear in bold. Normative values for CSF biomarkers were: Aβ42 >550 (pg.mL⁻¹), Tau <350 (pg.mL⁻¹), P-Tau <60 (pg.mL⁻¹), Aβ42/Aβ40 >0.055. P:pathological; N:Normal.

| | ALZ_441_005 | ALZ_596_006 | EXT_1998_001 | Case III-2 of [1] | EXT_2000_001 |
|--------------------|-------------|--------------------|--------------|-------------------|--------------|
| frontal cortex | 3R>4R | 4R>3R [#] | 4R | 4R | negative* |
| hippocampus | 3R>4R | 3R>4R | 3R/4R | 3R/4R | 4R* |
| enthorhinal cortex | 3R>4R | 3R>4R | 3R>4R | 3R/4R | 3R/4R |
| amygdala | 3R>4R | 3R>4R | 3R/4R | 4R > 3R | 4R |
| striatum | 3R | 3R | 4R | 4R >> 3R | 4R |
| Pallidum | 3R>>4R | 3R/4R | 4R | 4R >> 3R | 4R |
| SN | 3R>4R | 4R>3R | ND | 4R >> 3R | 4R |
| NBM | 3R>>4R | 3R>4R | 3R/4R | 3R/4R | 4R |
| Cerebellum | NA | 3R/4R | 4R | 4R | 4R |

Table 2. Distribution of 4R and 3R aggregates among brain regions in *MAPT* duplication carriers (patients ordered from right to left based on the main aggregated tau isoforms)

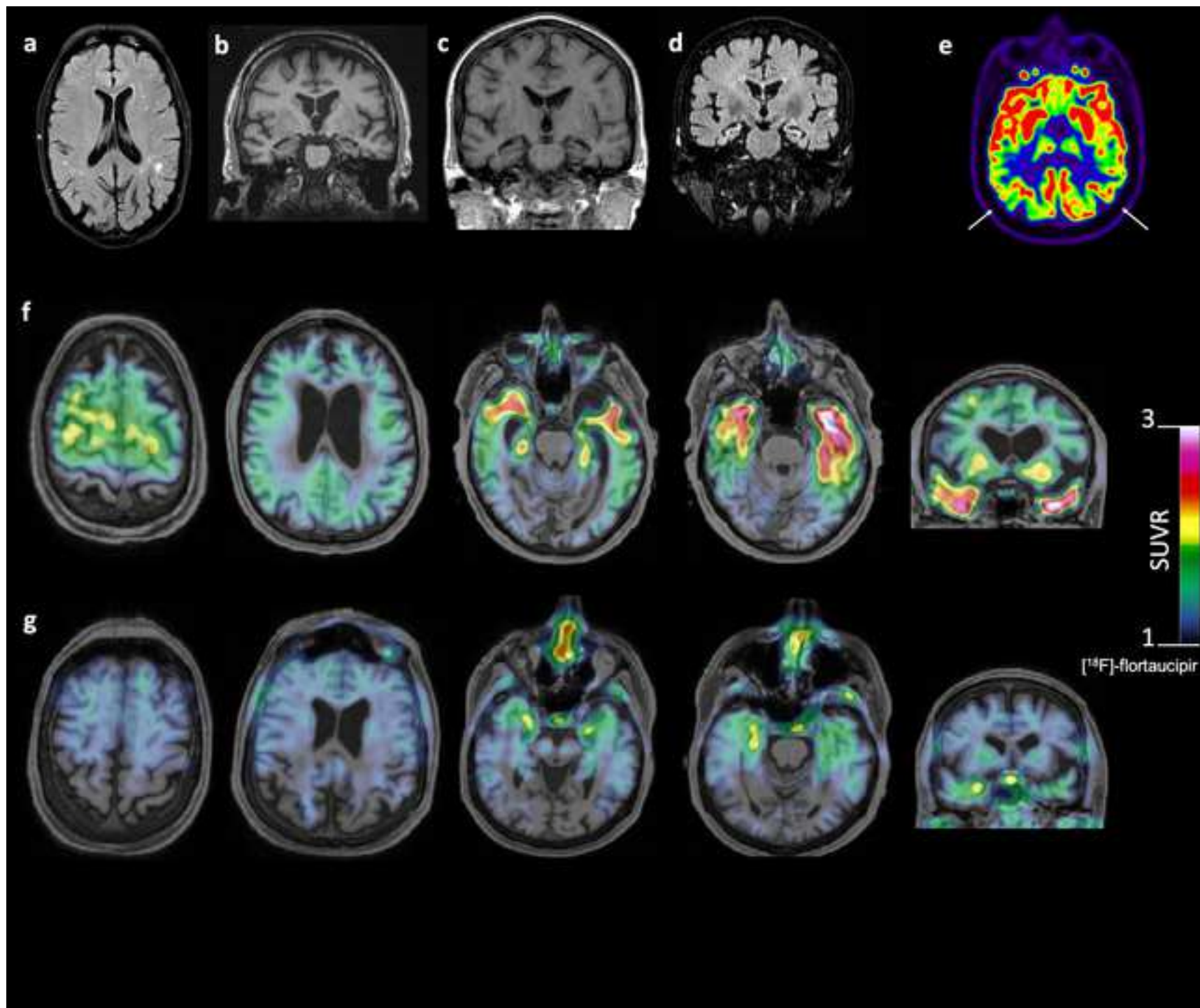
3R: positive immunostaining of 3R tau protein isoforms; 4R: positive immunostaining of 4R tau proteins isoforms. Case III-2 of [1]: immunohistochemistry data from the published case by Alexander et al., 2016 [1]; negative*: rare AT8-positive deposits which were negative for 3R and 4R staining; 4R*: rare AT8-positive deposits which were negative for 3R staining; 4R>3R[#]: In the frontal cortex 3R and 4R were similar in neurons but astrocytes were only positive for 4R. NA: not available.

REFERENCES

1. Alexander J, Kalev O, Mehrabian S, Traykov L, Raycheva M, Kanakis D, Drineas P, Lutz MI, Ströbel T, Penz T, Schuster M, Bock C, Ferrer I, Paschou P, Kovacs GG (2016) Familial early-onset dementia with complex neuropathologic phenotype and genomic background. *Neurobiol Aging* 42:199–204.
2. Bronner IF, Meulen BC ter, Azmani A, Severijnen LA, Willemsen R, Kamphorst W, Ravid R, Heutink P, Swieten JC van (2005) Hereditary Pick's disease with the G272V tau mutation shows predominant three-repeat tau pathology. *Brain* 128:2645–2653.
3. Caffrey TM, Joachim C, Paracchini S, Esiri MM, Wade-Martins R (2006) Haplotype-specific expression of exon 10 at the human MAPT locus. *Hum Mol Genet* 15:3529–3537.
4. Chen Z, Chen JA, Shatunov A, Jones AR, Kravitz SN, Huang AY, Lawrence L, Lowe JK, Lewis CM, Payan CAM, Lieb W, Franke A, Deloukas P, Amouyel P, Tzourio C, Dartigues JF, Groups N and BS, Ludolph A, Bensimon G, Leigh PN, Bronstein JM, Coppola G, Geschwind DH, Al-Chalabi A (2019) Genome-wide survey of copy number variants finds MAPT duplications in progressive supranuclear palsy. *Mov Dis* 34:1049–1059.
5. Clavaguera F, Bolmont T, Crowther RA, Abramowski D, Frank S, Probst A, Fraser G, Stalder AK, Beibel M, Staufenbiel M, Jucker M, Goedert M, Tolnay M (2009) Transmission and spreading of tauopathy in transgenic mouse brain. *Nat Cell Biol* 11:909–913.
6. Dan A, Takahashi M, Masuda-Suzukake M, Kametani F, Nonaka T, Kondo H, Akiyama H, Arai T, Mann DMA, Saito Y, Hatsuta H, Murayama S, Hasegawa M (2013) Extensive deamidation at asparagine residue 279 accounts for weak immunoreactivity of tau with RD4 antibody in Alzheimer's disease brain. *Acta Neuropathol Commun* 1:54.
7. Daude N, Kim C, Kang S-G, Eskandari-Sedighi G, Haldiman T, Yang J, Fleck SC, Gomez-Cardona E, Han ZZ, Borrego-Ecija S, Wohlgemuth S, Julien O, Wille H, Molina-Porcel L, Gelpi E, Safar JG, Westaway D (2020) Diverse, evolving conformer populations drive distinct phenotypes in frontotemporal lobar degeneration caused by the same MAPT-P301L mutation. *Acta Neuropathol* 139:1045–1070.
8. Dubois B, Feldman HH, Jacova C, Hampel H, Molinuevo JL, Blennow K, Dekosky ST, Gauthier S, Selkoe D, Bateman R, Cappa S, Crutch S, Engelborghs S, Frisoni GB, Fox NC, Galasko D, Habert M-O, Jicha GA, Nordberg A, Pasquier F, Rabinovici G, Robert P, Rowe C, Salloway S, Sarazin M, Epelbaum S, Souza LC de, Vellas B, Visser PJ, Schneider L, Stern Y, Scheltens P, Cummings JL (2014) Advancing research diagnostic criteria for Alzheimer's disease: the IWG-2 criteria. *Lancet Neurol* 13:614–629.
9. Furman JL, Holmes BB, Diamond MI (2015) Sensitive Detection of Proteopathic Seeding Activity with FRET Flow Cytometry. *J Vis Exp* doi: 10.3791/53205

10. Godefroy O, Azouvi P, Robert P, Roussel M, LeGall D, Meulemans T, Group G de R sur l'Evaluation des FES (2010) Dysexecutive syndrome: diagnostic criteria and validation study. *Ann Neurol* 68:855–864.
11. Holmes BB, Furman JL, Mahan TE, Yamasaki TR, Mirbaha H, Eades WC, Belaygorod L, Cairns NJ, Holtzman DM, Diamond MI (2014) Proteopathic tau seeding predicts tauopathy in vivo. *PNAS* 111:E4376-85.
12. Hooli BV, Kovacs-Vajna ZM, Mullin K, Blumenthal MA, Mattheisen M, Zhang C, Lange C, Mohapatra G, Bertram L, Tanzi RE (2014) Rare autosomal copy number variations in early-onset familial Alzheimer's disease. *Molecular Psy* 19:676–681.
13. Ingelsson M, Ramasamy K, Russ C, Freeman SH, Orne J, Raju S, Matsui T, Growdon JH, Frosch MP, Ghetti B, Brown RH, Irizarry MC, Hyman BT (2007) Increase in the relative expression of tau with four microtubule binding repeat regions in frontotemporal lobar degeneration and progressive supranuclear palsy brains. *Acta Neuropathol* 114:471–479.
14. Kovacs GG (2015) Invited review: Neuropathology of tauopathies: principles and practice. *Neuropathol. Appl. Neurobiol* 41:3–23.
15. Le Guennec K, Quenez O, Nicolas G, Wallon D, Rousseau S, Richard A-C, Alexander J, Paschou P, Charbonnier C, Bellenguez C, Grenier-Boley B, Lechner D, Bihoreau M-T, Olaso R, Boland A, Meyer V, Deleuze J-F, Amouyel P, Munter HM, Bourque G, Lathrop M, Frebourg T, Redon R, Letenneur L, Dartigues JF, Martinaud O, Kaley O, Mehrabian S, Traykov L, Ströbel T, Ber IL, Caroppo P, Epelbaum S, Jonveaux T, Pasquier F, Rollin-Sillaire A, Genin E, Guyant-Marechal L, Kovacs GG, Lambert JC, Hannequin D, Campion D, Rovelet-Lecrux A (2017) 17q21.31 duplication causes prominent tau-related dementia with increased MAPT expression. *Molecular Psy* 22:1119–1125.
16. Lesné S, Koh MT, Kotilinek L, Kaye R, Glabe CG, Yang A, Gallagher M, Ashe KH (2006) A specific amyloid-beta protein assembly in the brain impairs memory. *Nature* 440:352–357.
17. Marquié M, Normandin MD, Vanderburg CR, Costantino IM, Bien EA, Rycyna LG, Klunk WE, Mathis CA, Ikonovic MD, Debnath ML, Vasdev N, Dickerson BC, Gomperts SN, Growdon JH, Johnson KA, Frosch MP, Hyman BT, Gómez-Isla T (2015) Validating novel tau positron emission tomography tracer [F-18]-AV-1451 (T807) on postmortem brain tissue. *Ann Neurol* 78:787–800.
18. Myers AJ, Pittman AM, Zhao AS, Rohrer K, Kaleem M, Marlowe L, Lees A, Leung D, McKeith IG, Perry RH, Morris CM, Trojanowski JQ, Clark C, Karlawish J, Arnold S, Forman MS, Deerlin VV, Silva R de, Hardy J (2007) The MAPT H1c risk haplotype is associated with increased expression of tau and especially of 4 repeat containing transcripts. *Neurobiol Dis* 25:561–570.
19. Neumann M, Schulz-Schaeffer W, Crowther RA, Smith MJ, Spillantini MG, Goedert M, Kretschmar HA (2001) Pick's disease associated with the novel Tau gene mutation K369I. *Ann Neurol* 50:503–513.

20. Rösler TW, Marvian AT, Brendel M, Nykänen N-P, Höllerhage M, Schwarz SC, Hopfner F, Koeglsperger T, Respondek G, Schweyer K, Levin J, Villemagne VL, Barthel H, Sabri O, Müller U, Meissner WG, Kovacs GG, Höglinger GU (2019) Four-repeat tauopathies. *Prog Neurobiol* 180:101644.
21. Rovelet-Lecrux A, Hannequin D, Guillin O, Legallic S, Jurici S, Wallon D, Frebourg T, Campion D (2010) Frontotemporal dementia phenotype associated with MAPT gene duplication. *JAD* 21:897–902.
22. Sahara N, Kimura T (2018) Biochemical Properties of Pathology-Related Tau Species in Tauopathy Brains: An Extraction Protocol for Tau Oligomers and Aggregates. *Methods Mol. Biol.* 1779:435–445.
23. Sarazin M, Berr C, Rotrou JD, Fabrigoule C, Pasquier F, Legrain S, Michel B, Puel M, Volteau M, Touchon J, Verny M, Dubois B (2007) Amnestic syndrome of the medial temporal type identifies prodromal AD: a longitudinal study. *Neurology* 69:1859–1867.
24. Scheltens P, Barkhof F, Leys D, Pruvo JP, Nauta JJ, Vermersch P, Steinling M, Valk J (1993) A semiquantitative rating scale for the assessment of signal hyperintensities on magnetic resonance imaging. *J Neurol Sci* 114:7–12
25. Sierra M, Martínez-Rodríguez I, Sánchez-Juan P, González-Aramburu I, Jiménez-Alonso M, Sánchez-Rodríguez A, Berciano J, Banzo I, Infante J (2017) Prospective clinical and DaT-SPECT imaging in premotor LRRK2 G2019S-associated Parkinson disease. *Neurology* 89:439–444.
26. Tacik P, DeTure MA, Carlomagno Y, Lin W, Murray ME, Baker MC, Josephs KA, Boeve BF, Wszolek ZK, Graff- Radford NR, Parisi JE, Petrucelli L, Rademakers R, Isaacson RS, Heilman KM, Petersen RC, Dickson DW, Kouri N (2017) FTDP- 17 with Pick body- like inclusions associated with a novel tau mutation, p.E372G. *Brain Pathol* 27:612–626.
27. Thierry M, Boluda S, Delatour B, Marty S, Seilhean D, Network BN-CN, Potier M-C, Duyckaerts C (2020) Human subiculo-fornico-mamillary system in Alzheimer’s disease: Tau seeding by the pillar of the fornix. *Acta Neuropathol* 139:443–461.
28. Trabzuni D, Wray S, Vandrovicova J, Ramasamy A, Walker R, Smith C, Luk C, Gibbs JR, Dillman A, Hernandez DG, Arepalli S, Singleton AB, Cookson MR, Pittman AM, Silva R de, Weale ME, Hardy J, Ryten M (2012) MAPT expression and splicing is differentially regulated by brain region: relation to genotype and implication for tauopathies. *Hum Mol Genet* 21:4094–4103.
29. Uchihara T, Kondo H, Ikeda K, Kosaka K (1995) Alzheimer-type pathology in melanin-bleached sections of substantia nigra. *J Neurol* 242:485–489.
30. Yamamoto T, Hirano A (1986) A comparative study of modified Bielschowsky, bodian and thioflavin S stains on Alzheimer’s neurofibrillary tangles. *Neuropath Appl Neuro* 12:3–9.



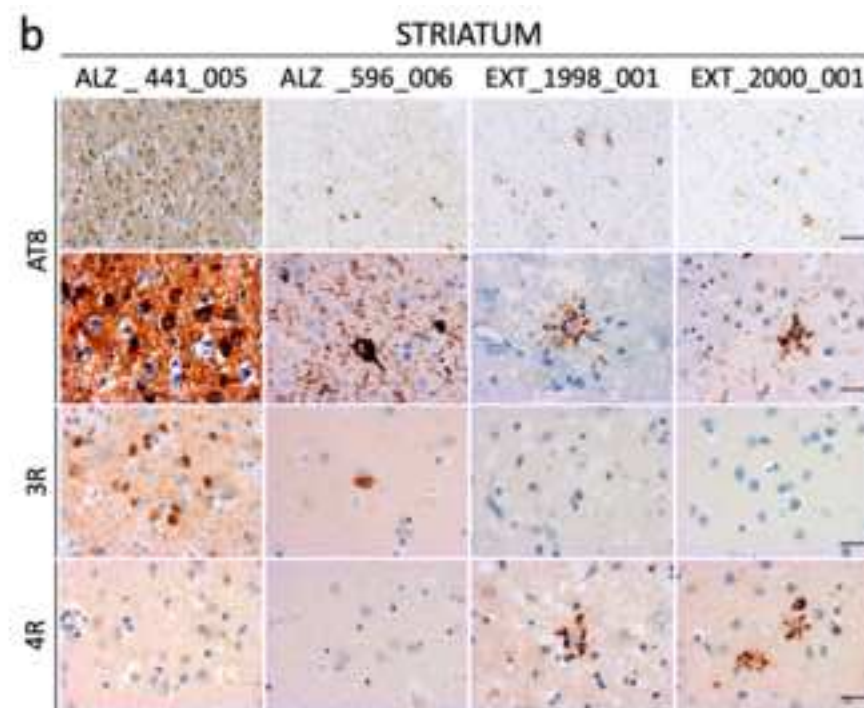
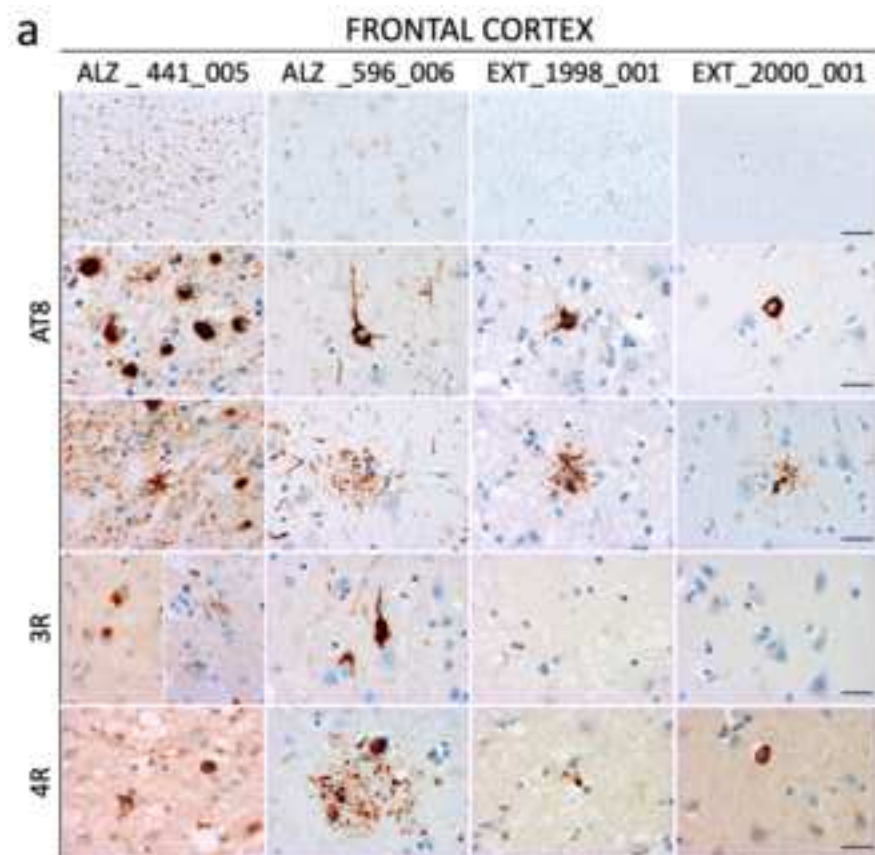


Fig 3_HR.tiff

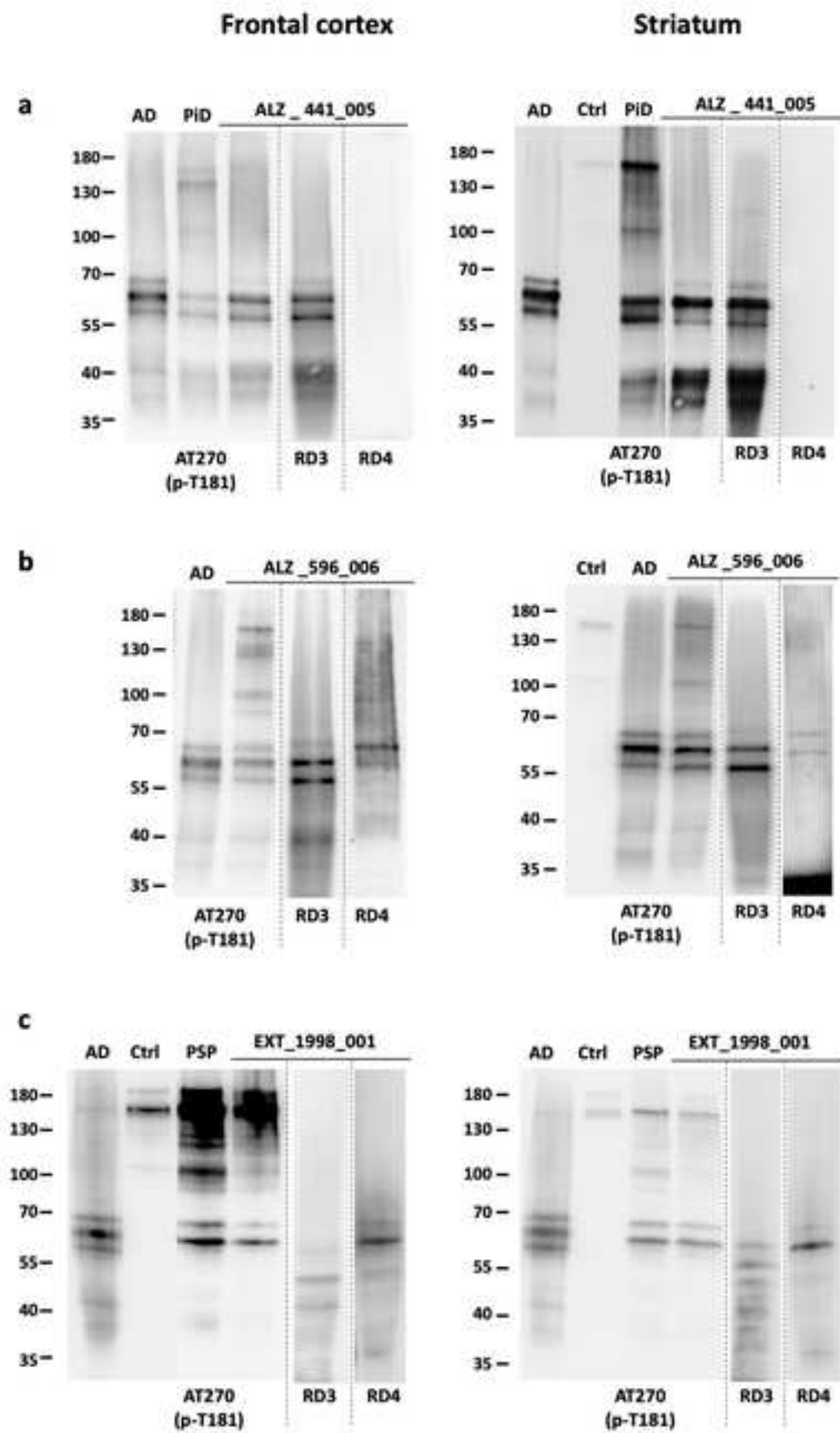
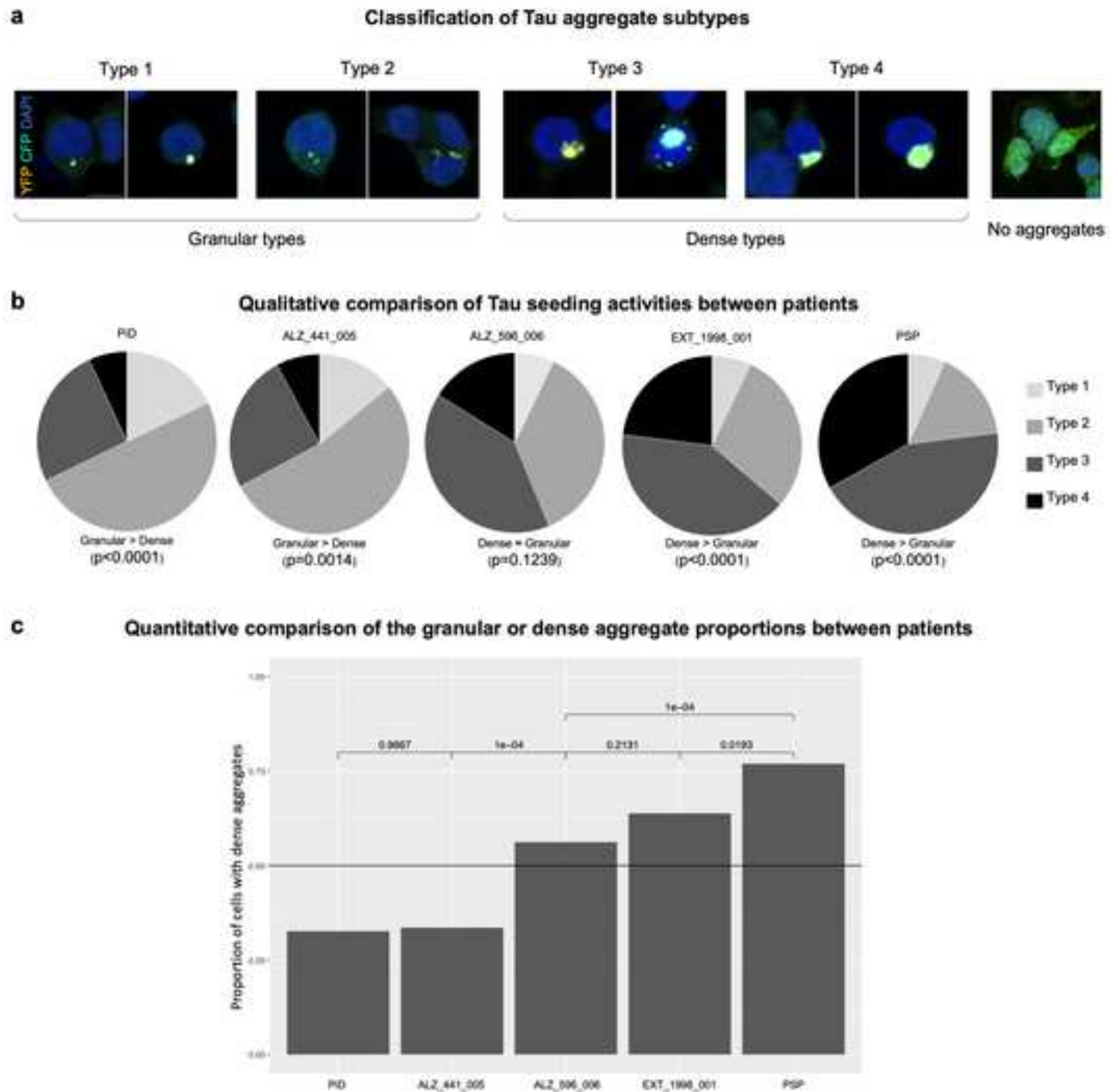


Figure 4.tiff



[Click here to view linked References](#)



Click here to access/download
attachment to manuscript
Supplementary Fig. 1.tiff





Click here to access/download
electronic supplementary material
Supplementary Fig. 2.tiff





Click here to access/download
electronic supplementary material
Supplementary Fig. 3.tiff





Click here to access/download
electronic supplementary material
Supplementary Fig. 4.tiff





Click here to access/download
electronic supplementary material
Supplementary Fig. 5.tiff





Click here to access/download
electronic supplementary material
Supplementary Fig. 6.tiff





Click here to access/download
electronic supplementary material
Supplementary Fig. 7.tiff





Click here to access/download

electronic supplementary material

Supplementary Table 1_Table 3R 4R p62 AT100 G
B.docx